Journal of Materials Chemistry B

ROYAL SOCIETY OF CHEMISTRY

REVIEW

View Article Online
View Journal | View Issue

Cite this: J. Mater. Chem. B, 2023, 11, 5321

Organized mineralized cellulose nanostructures for biomedical applications

Yanhuizhi Feng,[a] Helmut Cölfen *[b] and Rui Xiong *[c]

Cellulose is the most abundant naturally-occurring polymer, and possesses a one-dimensional (1D) anisotropic crystalline nanostructure with outstanding mechanical robustness, biocompatibility, renewability and rich surface chemistry in the form of nanocellulose in nature. Such features make cellulose an ideal bio-template for directing the bio-inspired mineralization of inorganic components into hierarchical nanostructures that are promising in biomedical applications. In this review, we will summarize the chemistry and nanostructure characteristics of cellulose and discuss how these favorable characteristics regulate the bio-inspired mineralization process for manufacturing the desired nanostructured bio-composites. We will focus on uncovering the design and manipulation principles of local chemical compositions/constituents and structural arrangement, distribution, dimensions, nanoconfinement and alignment of bio-inspired mineralization over multiple length-scales. In the end, we will underline how these cellulose biomineralized composites benefit biomedical applications. It is expected that this deep understanding of design and fabrication principles will enable construction of outstanding structural and functional cellulose/inorganic composites for more challenging biomedical applications.

Received 30th November 2022,
Accepted 25th January 2023

DOI: 10.1039/d2tb02611b

rsc.li/materials-b

10th Anniversary Statement

Journal of Materials Chemistry B is certainly among the first choices when publishing cutting-edge research in the field of bionic/bioinspired materials is considered. With the aging society as one of the grand human challenges, bio-inspired materials with medical applications are of rapidly increasing importance and need. Among other related topics, this journal contains a good mix of important research work, authoritative reviews and perspectives in this research field. Therefore, we congratulate the *Journal of Materials Chemistry B* for 10 years of successful publication and presentation of exciting research in this area and wish all success for further advancement of the journal. It will be nice to see further key findings in the field published here.

1. Introduction

Natural structural mineralized materials created by living creatures are usually composed of stiff minerals and soft biopolymers that are organized into multi-dimensional hierarchical architectures.[1,2] For instance, teeth and bones are essentially comprised of hydroxyapatite (HAp) and collagen with a highly aligned one-dimensional (1D) structure to obtain outstanding load bearing capability.[3] Nacres utilize aragonite microplates and chitin/silk protein to build a two-dimensional (2D) brick-mortar architecture to overcome the trade-off between toughness and strength.[4] Crustacean exoskeletons evolve amazing damage-tolerant properties through the growth of crystalline/amorphous calcium carbonate into chitin/silk protein three-dimensional (3D) twisted plywood structures.[5,6] These complex structural designs and excellent biological interfaces endow natural structural materials with fascinatingly high strength, high stiffness, high toughness, and on-demanded functionalities.[7] By learning these natural processes, the nucleation, growth, and assembly process of inorganic minerals can be regulated by artificial organic templates, and ordered nanostructures like cartilage, teeth and nacre and can be precisely synthesized, thereby realizing the excellent structural properties and functionalities of these materials.[8–11] Thus, biomimetic mineralization is an important strategy to construct high-performance structural and functional materials,[12–15] especially for biomedical applications, since natural biomineralized materials are usually used as the essential structural and functional tissues in living creatures.

[a] Department of Periodontology, Stomatological Hospital and Dental School of Tongji University, Shanghai Engineering Research Center of Tooth Restoration and Regeneration, Shanghai 200072, China
[b] Physical Chemistry, Department of Chemistry, University of Konstanz, Universitätsstraße 10, Konstanz, Germany. E-mail: helmut.coelfen@uni-konstanz.de
[c] State Key Laboratory of Polymer Materials Engineering, Polymer Research Institute of Sichuan University, Chengdu, 610065, China. E-mail: rui.xiong@scu.edu.cn

To mimic natural hierarchical architectures, the selection of organic building-blocks/templates is critical due to the importance of interface design and bio-enabled concerns in biomedical applications. Compared with synthetic polymers, biopolymers usually demonstrate the following advantages: (i) good biocompatibility, biodegradability, renewability, and rich surface chemistry, which are essentially important for the biomedical applications;[16] (ii) self-assembly of ordered secondary nanostructures to greatly enrich the structural hierarchy;[17] and (iii) chemical and structural ingredient similarity with these natural counterparts for obtaining good structural and functional properties.[18]

Cellulose is the most abundant naturally-derived biopolymer on earth with an annual production of 100 billion tons.[19] It is synthesized by a large number of living organisms, including plants, algae/fungi, and bacteria, and comprises the major structural component of their cell walls.[20] This naturally-occurring cellulose is in the form of nanofibers with linear molecular chains highly aligned together, thus gaining outstanding mechanical robustness that is comparable to Kevlar fibers.[19] The structural hierarchy of cellulose at a multi-length scale ranging from the molecular level to nanoscale and microscale, and to the macroscopic level, facilitates the preparation of the various forms of cellulose at different length scales, including molecular solution, nanofibers/nanocrystals, and microfibers. These multi-scaled cellulose forms combined with tailorable surface chemistry are ideal bio-building blocks to construct mineralized materials with hierarchical organizations that closely mimic those that have been built by living creatures. The development of cellulose based mineralized materials from renewable and sustainable resources would have great potential as next-generation sustainable bio-enabled composites that have a low environmental impact and low safety risks to human health. Cellulose and cellulosic materials have distinguished properties for future multi-applications. (Table 1).

Although studies to develop cellulose as a new advanced material have tremendously progressed in recent decades,[27] controlling the biomineralization process as precisely as intricate biological systems remains a grand challenge. To apply cellulose based mineralized materials as ecofriendly high-performance biomedical materials, it is vital to understand how to utilize the surface chemistry and nanostructure characteristics of cellulose to regulate the biomineralized architectures with long-range order. The biomimetic hierarchical architectures are key in the optimal expression of minerals and cellulose properties, and further functionalities due to their synergistic toughening mechanisms. However, existing

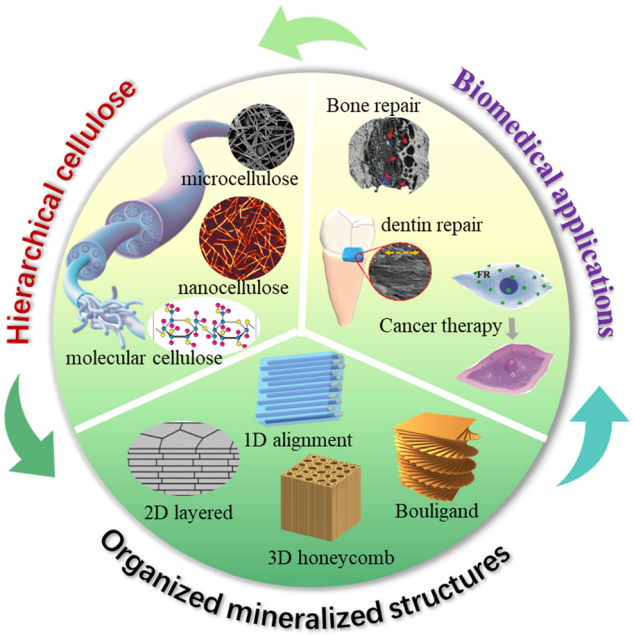

Fig. 1 Overview of the organized mineralized cellulose structures for biomedical applications.

reviews rarely systematically discuss the related design and fabrication principles based on organized mineralized cellulose structures,[28–30] and therefore we have written this review to address this issue. We summarize the chemistry and nanostructure characteristics of cellulose at multi-length scale and discuss how these favorable characteristics regulate the bio-inspired mineralization process for manufacturing highly ordered nanostructured biocomposites in multiple dimensions. The underlying mechanical and functional enhancement mechanisms are carefully discussed, and we highlight how these properties benefit biomedical applications (Fig. 1). It is expected that this deep understanding of design and fabrication principles will lead to the construction of outstanding structural and functional nanocellulose/inorganic composites for more challenging biomedical applications.

2. Cellulose at the molecular-, nano-, and micro-scales

Cellulose is a linear polymer composed of several hundreds to thousands of glucose units that are joined by β-1,4 linkages. During biosynthesis, strong hydrogen bonding and van der Waals forces lead to parallel packing of multiple cellulose

Table 1 Comparison of molecular cellulose, nanocellulose, and mineralized cellulose

Criteria	Molecular cellulose	Nanocellulose	Mineralized cellulose
Stability	Chemically modifiable[21]	Chemically modifiable[21]	Chemically modifiable[22]
Flexibility	Good[23]	Good	Good[24]
Raw materials price	Low cost[20]	Low cost[20]	Low cost[20]
Mass production capability	Commercially available[25]	Commercially available[25]	Non-commercially available[26]

molecular chains to form elementary nanofibrils with a diameter of 2–3 nm, which further bundle into larger microfibrils with a diameter of 5–50 nm.[31] The highly ordered anisotropic arrangement and strong intra- and inter-chain interactions make cellulose water-insoluble and provide cellulose fibers with a high axial strength and stiffness.[32] The hierarchical structure of cellulose in nature is finely controlled through biosynthesis and assembly, resulting in an infinite number of structural differences across cellulosic species. These structural variations lead to numerous structural–functional diversities, such as the combination of lightweight and exceptional mechanical properties in wood, and brilliant structural colors in many flowers and fruits.[7,33] Wood is the most typical example of the construction of cellulose into a complex hierarchical structure in nature. Native cellulose is a semicrystalline 1D fibril material consisting of crystalline (microfibers or rodlike entities) and amorphous regions, which are embedded in an amorphous matrix of hemicellulose and lignin to constitute the plant cell wall.[34] These cellulose fibrils are usually oriented along the axial direction of wood to optimize the load bearing properties that could protect their living bodies against biological attack and external stress.[35] Overall, cellulose possesses a structural hierarchy at different length scales, including linear chains at the molecular scale, nanofibers/crystals at the nanoscale, and microfibers at the microscale (Fig. 2(a)),[36] which eventually build up the hierarchical structures of living organisms.

2.1 Molecular cellulose

Molecular cellulose mainly refers to the cellulose or cellulose derivatives solution, which can be utilized to fabricate regenerated cellulose. Regenerated cellulose is a class of cellulosic materials manufactured by cellulose dissolution and subsequent regeneration. Various forms of regenerated cellulose, including fibers, films, and hydrogels, can be fabricated by wet spinning, drop-casting, and molding of cellulose/cellulose derivative solutions, followed by a regeneration process of solvent evaporation or coagulation bath.[37–39] Cellulose is insoluble in conventional polar/non-polar solvents due to the long-length molecular chains and strong chain interactions due to hydrogen bonds. Only some specific solvents, including $NaOH/CS_2$, *N*-methylmorpholine-*N*-oxide (NMMO), LiCl/*N*,*N*-dimethylacetamide, ionic liquids (ILs) and alkali/urea *etc.*, have been developed to dissolve cellulose through disrupting these hydrogen bonds.[40] However, some of these solvents (such as $NaOH/CS_2$ and NMMO) cause serious environmental problems so they have been gradually replaced by more ''green'' solvents (*e.g.* ILs and alkali/urea) in applications.[41–44]

To make cellulose water soluble, esterification and etherification of cellulose is the main strategy. Many cellulose esters and ethers, such as methylcellulose (MC), hydroxypropyl cellulose (HPC), and carboxymethyl cellulose (CMC), are water-soluble polymers, which have already been commercially available for decades. The water solubility highly depends on the degree of substitution (DS) of hydroxyl groups on the cellulose chains. A high DS can significantly weaken the hydrogen bonding to give cellulose good water solubility and even solubility in polar organic solvents.[45] Interestingly, some cellulose derivatives are temperature sensitive. For example, HPC aqueous solutions exhibit an unusual solubility behavior with good solubility in cold water, but insolubility in hot water, resulting in the gelation of cellulose chains.[46] The transition temperature can be manipulated by controlling the ratio of

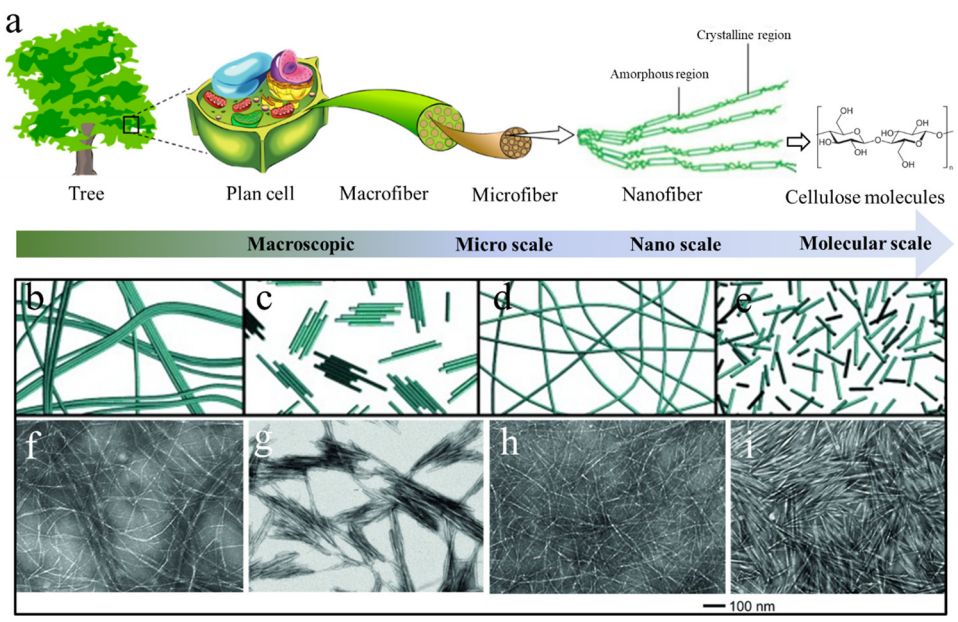

Fig. 2 (a) The hierarchical cellulose structure in plants and trees at different length scales. Reprinted from ref. 36 with permission from DMPI, copyright 2020. (b)–(i) Schematic illustration and corresponding TEM images of nanocellulose materials prepared from wood pulp using different methods: (b) and (f) CNFs prepared by high-intensity ultrasonication; (c) and (g) CNCs prepared by HCl hydrolysis; (d) and (h) CNFs prepared by TEMPO pretreatment and ultrasonication; (e, i) CNCs prepared by H_2SO_4 hydrolysis. Reprinted from ref. 50 with permission from Wiley, copyright 2014.

hydroxypropyl substitutions. This unique temperature-sensitivity is highly attractive for the design and fabrication of temperature responsive biocomposites.

2.2 Nanocellulose

Nanocellulose is a form of one-dimensional nanosized cellulose fibers with a diameter <100 nm. It combines the desirable intrinsic properties of cellulose (*e.g.*, renewability, biocompatibility, biodegradability, and low density) with the features of nanomaterials, including high strength (~7 GPa) and stiffness (110–220 GPa), high-aspect-ratio, high specific surface area, reinforcing capabilities, and self-assembly behavior in aqueous media.[47] These outstanding properties make nanocellulose a rising star in the materials science field including applications. Nanocelluloses can be categorized into cellulose nanofibers (CNFs), cellulose nanocrystals (CNCs), and bacterial cellulose (BC) depending on their morphologies and sources.

Elementary CNFs are the smallest element next to cellulose molecules with a diameter of 2–3 nm and length of several-micrometers.[48] They consist of fully extended cellulose chains closely packed along the longitudinal direction with alternatively highly ordered crystalline and amorphous regions. CNFs can be exfoliated from cellulosic sources through various intensive mechanical disintegration techniques, such as ultrasonication, a high-pressure homogenizer, grinder, ball mill *etc.*[49] However, CNFs directly obtained from these techniques usually show a large diameter distribution and poor aqueous dispersibility (Fig. 2(b) and (f)),[50] resulting in the semi-transmittance or non-transmittance of the dispersion and films. To prepare uniform elementary CNFs with good aqueous stability, pre-chemical treatments of cellulose have to be conducted to introduce significant amounts of charged groups on the cellulose microfiber surfaces. C6-carboxylation of cellulose by 2,2,6,6-tetramethylpiperidine-1-oxyl (TEMPO) pretreatments is the most widely used approach to gain homogeneous and stable CNF aqueous dispersions.[51] The grafted negatively charged carboxyl groups during TEMPO treatment can produce strong electrostatic repulsion between cellulose microfibers.[52] Consequently, using mild mechanical disintegration can break all the interfibrillar hydrogen bonds between cellulose microfibrils and obtain completely individualized elementary CNFs dispersed in water (Fig. 2(d) and (h)),[50] which can significantly reduce energy consumption in the mechanical disintegration process.[53]

CNCs can form rigid rod-like nanocellulose with diameters in the range 3–50 nm and lengths of 50–500 nm depending on the cellulosic source and preparation methods.[54] Strong acid hydrolysis of cellulose preferentially etches the amorphous regions of cellulose microfibers to liberate CNCs. The CNCs prepared by sulfuric acid hydrolysis show excellent aqueous stability due to the sulfate groups grafting during the sulfuric acid hydrolysis (Fig. 2(e) and (i)), while HCl treated CNCs usually aggregate together and show poor dispersion stability due to the absence of surface charges (Fig. 2(c) and (g)).[50] In contrast to the uniform and smooth elementary CNFs, CNCs in most cases have spindle-like morphologies with larger diameters because of the presence of large crystal bundles. Intensive ultrasonication treatment of the CNC dispersion can separate their bundles into individual CNCs with a large decrease in the CNCs size.[55] As a result, the white, turbid, or translucent CNC dispersion turned into a transparent blueish dispersion. Interestingly, CNCs are capable of self-organizing into a chiral nematic (cholesteric) liquid crystal (LC) phase with a helical arrangement when the CNC dispersion is above a critical concentration.[56] Upon drying, the chiral nematic LC phase is saved in the solid-state film with a striking iridescent structural color because of Bragg reflection of visible light from dried films.[57] Unlike the traditional structural colors from photonic crystals and layered structures, the more complex internal structure of CNC LC films adds the structural color sensitivity to circular polarization, which shares similarities with the brilliant structural color produced by the twisted plywood structure of fruits and beetles.[58]

BC can be produced by bacteria fermentation (such as *A. xylinum, A. hansenii, and A. pasteurianus*) with the form of hydrogel-like pellicles by cultivating in an aqueous culture medium for a few days.[59,60] Compared to nanocellulose from plants, BC has a more crystalline structure, and is more chemically pure without hemicellulose or lignin that often exists in CNFs. The high polymerization degree and ultrafine network architecture also makes BC stronger and tougher than other types of nanocellulose based materials. However, the distinct ribbon-like 3D network structure with a large diameter of around 100 nm makes the dried BC film only semi-transparent.

2.3 Cellulose microfibers

Original cellulose in plants usually exists in the form of cellulose microfibers, together with hemicellulose and lignin constituents in the cell walls of plants, which is one of the most ancient raw materials that human beings have developed for making paper. Through pulping processes, such as mechanical, semi-chemical or fully chemical methods (kraft and sulfite processes), individual cellulose microfibers can be isolated from plants. The original hollow structure of cellulose microfibers is usually flattened after the pulping process due to the collapse of the lumen during mechanical treatments and subsequent drying.[61] The size of the microfibers depends on the cellulosic sources with a usual width of 10–50 microns and length of several millimeters. Compared with nanocellulose, cellulose microfibers are more cost-efficient and more porous. The large diameter size also makes them suitable for use as a bio-template for nano/micro-particle assembly or growth. Additionally, cellulose microfibers can be made into paper though well-established industrial paper-making processes for various applications, ranging from their ancient application for writing to emerging applications in flexible electronic devices, biomedicines, energy harvesting and storage.[62–64]

3. Mineralized cellulose materials at multiple dimensions

The structural diversity of cellulose provides numerous possibilities to arrange it with functional inorganic components to

construct advanced structural and functional composites with high structural complexity. Considering the significant diversity of synthetic mineralized materials, appropriate classification of the material microstructures presents an important step toward a comprehensive understanding of design and fabrication strategies for architected materials. These efforts to produce mineralized cellulose composites can be categorized into three major groups (1D, 2D and 3D) according to the dimensional diversity of their architectures. In this section, we selectively focus on the construction of mineralized cellulose materials with well-defined order and the unique enhancement of their mechanical properties and functionalities.

3.1 One dimensional (1D) individual fibril/aligned nanofibril structures

3.1.1 Individual fibril structure. Cellulose possesses one dimensional fibril structures at the nano/micro scale, which is an ideal biotemplate for the growth of inorganic components on the fibrils surface to form hierarchical core/shell architectures. To date, a wide range of inorganic nanoparticles (NPs) are decorated on cellulose fiber surfaces from random decoration to conformal wrapping around dense layers through *in situ* growth and self-assembly.

In situ growth. In situ growth of mineral NPs decorated on cellulose nanofibers ensures uniform NP distribution, thereby avoiding the traditional mixing stage with the potential risk of particle agglomeration. Cellulose fiber (CF) paper is a low-cost, sustainable, and flexible substrate that can be assembled from cellulose microfibers using paper-making techniques. The highly porous network, large surface area and rich surface chemistry of cellulose microfibers provide abundant bonding sites for direct mineralization. Great progress has been achieved in functionalizing CF paper by the *in situ* growth of inorganic particles to meet the requirements of specific applications. For instance, ultralong HAp nanowires (HAPNWs) with lengths larger than 10 μm have been demonstrated to radially grow on cellulose microfibers (Fig. 3(a)).[65] This unique micro/nanoscale hierarchical structure can be easily customized by Eu^{3+}/Tb^{3+} ion doping and poly(dimethylsiloxane) coating for added photoluminescence and superhydrophobicity. Additionally, zinc oxide (ZnO) nanowires can also be incorporated on the fiber surfaces to form a similar core/shell structure through well-established hydrothermal methods.[66,67] Metal–organic frameworks (MOFs) are emerging nanomaterials that are of great interest with diverse applications in gas separation, catalysis, energy, environmental science, and biomedicine, due to their large specific surface areas, high porosities, and rich functionality. However, the difficulty in processing MOF crystals and controlling the MOF superstructure limits their applications. Li and Yu *et al.*[68,69] have demonstrated that the 1D nanofibril morphology of CNF and the negatively charged surface chemistry could shift the balance of nucleation and growth towards synthesizing smaller MOF crystals, and further decreased their aggregation possibilities. Furthermore, CNF can provide extrinsic porosity, mechanical flexibility, and easy-processability for the resultant composites due to the hybrid core/shell structure.

In addition to the nanowires and MOFs, various types of functional mineral nanospheres (*e.g.* noble metal NPs and magnetic NPs) have been widely *in situ* grown on cellulose nano/micro fiber surfaces for on-demand functionality. Interestingly, noble metal NPs, including gold, silver and palladium, could be directly deposited on nanocellulose using nanocellulose as a reducing agent and stabilizing template under hydrothermal conditions, due to the abundant electron-rich hydroxyl groups on the cellulose surface.[70–74] This process is not only green without introducing extra toxic reducing agents, but also enables superior catalytic performance of the immobilized metal NPs.[70] Conventional soft reducing or stabling agents of metal NPs, such as polyvinylpyrrolidone (PVP) and polyethylene glycol (PEG), usually densely wrap around the NPs surface, which significantly shields the interaction with other components, leading to deteriorated performance, such as catalysis and conductivity. By contrast, the reduction and stabilization of NPs by stiff nanocellulose could expose more active sites to external environments for favorable interaction and thus for enhanced performance. However, the approach is difficult to realize for high loading of metal NPs due to the limited reduction ability of nanocellulose. To achieve high decoration of NPs, additional reduction agents are usually needed to pre-assemble on the nanocellulose surface. For example, bio-inspired polydopamine (PDA) has been used to *in situ* grow and immobilize Ag NPs on the nanocellulose surface.[75] Magnetic NPs have been *in situ* grown on cellulose fibril templates for adding magnetic functionalities, respectively.[76–78] These inorganic-bio hybrids could be further assembled into flexible solid magnetic bio-films.[79] In a recent study, a uniform layer of amorphous calcium carbonate in the form of small beads was demonstrated to grow on the CNF surface to form a core–shell structure using a binary water/organic solvent.[80]

Self-assembly. Interfacial interaction leading to self-assembly of nanocellulose with functional NPs is another approach to introduce NPs on the nanocellulose templates. The abundance of hydroxyl, carboxyl, and sulfate groups on the surface of the nanoparticle/fibril allows the generation of supramolecular interactions with functional NPs, such as hydrogen bonding, electrostatic interaction, and van der Waals forces. Majoinen *et al.*, used the electrostatic interaction between cationic gold NPs (AuNPs) and anionic CNC to assemble AuNPs on the surfaces of individualized CNC colloidal rods (Fig. 3(b)).[81] The right-handed twist along individual CNC templates and the chiral twisted assembly of AuNPs along their axis, led to a chiral plasmonic response on the nanoscale. CdSe/ZnS quantum dots (QDs) have also been demonstrated to be successfully decorated around carboxylated CNCs using a carbodiimide chemistry coupling approach.[82] The QD–CNC hybrids exhibit colloidal stability in aqueous suspension and provide strong fluorescence to a CNC film with low NP loading, maintaining the overall physical properties or self-assembly of the CNCs.[82] Anionic nanodiamond nanoparticles could also be used to

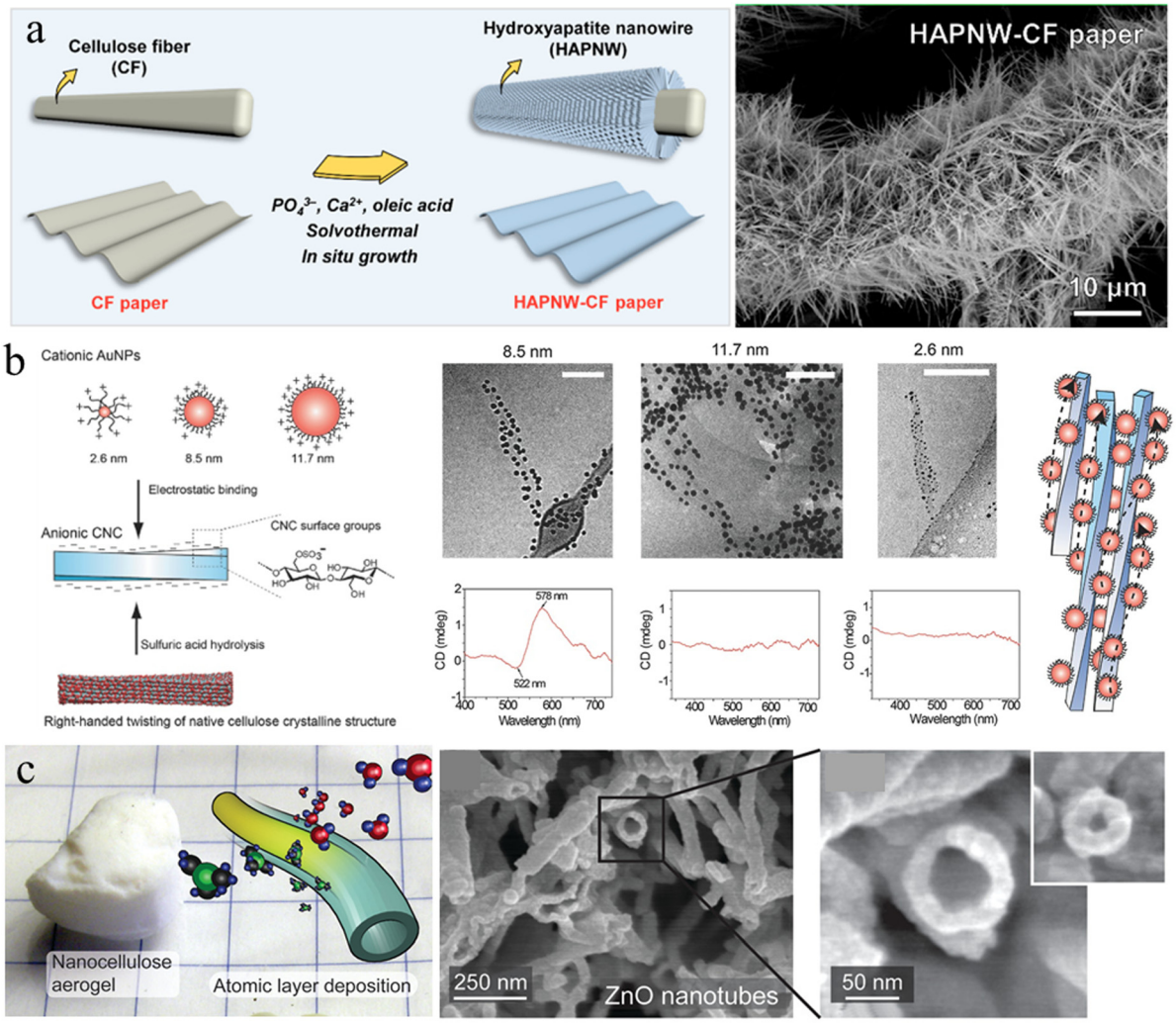

Fig. 3 (a) Schematic representation of the *in situ* growth of HAp nanowires on a cellulose microfiber surface and the corresponding SEM image. Reprinted from ref. 65 with permission of the American Chemical Society, copyright 2021. (b) Scheme for electrostatic binding of plasmonic AuNPs onto CNCs for chiral plasmonics in dilute aqueous dispersion, and Cryo-TEM images and circular dichroism measurements upon electrostatic binding of AuNP onto CNC. Reprinted from ref. 81 with permission of Wiley, copyright 2016. (c) Inorganic hollow nanotubes prepared from the nanocellulose aerogel by the ALD and subsequent calcination. Reprinted from ref. 92 with permission of the American Chemical Society, copyright 2021.

successfully decorate cationic CNFs in hydrocolloidal form for greatly hardening cellulose materials.[83] Additionally, nanocellulose was recently demonstrated to be an amphiphilic biofibril due to the highly ordered and dense packing of cellulose molecular chains.[84–86] The OH groups decorate hydrophilic planes, while CH groups constitute hydrophobic planes.[87] This unique amphiphilic behavior can be utilized to assemble and disperse hydrophobic nanocarbon materials and minerals, such as carbon nanotubes, nanodiamonds, graphene and boron nitride.[88,89] These NPs stabilized by nanocellulose could be used to further construct robust and functional bio-enabled nanomaterials.

Atomic layer deposition (ALD). ALD is a sequential, self-limiting chemical vapor deposition method used to deposit an ultrathin, conformal and homogenous layer on various substrates, which enables precise control of the desired film thickness by the number of deposition cycles.[90] Due to the easy operation, good reproducibility and high conformality of the as-deposited layer, ALD appears to be a promising technique for the deposition of inorganic layers on nanocellulose templates. Porous nanocellulose aerogels possess good mechanical strength and flexibility to ensure the structural integrity under the high vacuum conditions of ALD. Additionally, the complex porosity of the aerogels produces a large surface area for the gas phase of ALD reactions to fully saturate the nanocellulose network surface.[91] Korhonen *et al.* reported that the highly porous percolating network of nanocellulose aerogel produced by supercritical drying is an ideal biological nanofibrillar template for ALD.[92] Uniform oxide layers (titanium dioxide, zinc oxide, and aluminum oxide) have been deposited on the cellulose nanofiber surface to form an organic–inorganic core/shell structure with shell thickness down to <3 nm. Subsequent calcination at 450 °C to remove the cellulose core results

in inorganic self-supporting aerogels consisting of hollow nanotubular networks (Fig. 3(c)). Similarly, Li *et al.* demonstrated that 3D TiO_2 fiber-nanorod (NR) heterostructures can be prepared by the ALD assisted ZnO-coated CNF template and subsequent TiO_2 NRs growth.[93]

3.1.2 Aligned nanofibril structure. In nature, many structural materials gain mechanical robustness by taking advantage of the reinforcing mechanism of highly aligned nanofibril structures, such as bone and tooth dentin. Human bone is one of the most intriguing examples as it serves as a damage-tolerant structural framework, stemming from its hierarchical structure.[3] In this structure, the mineralized aligned collagen nanofibers are the basis of these hard tissues. At the nanoscale, highly aligned and stiff collagen triple helices pack together in a defined pattern dictated by the protein–protein interactions forming a collagen fibril, while the mineral platelets grow in the gap zones between the heads and tails of the collagen molecules as well as the fibril surface, where the *c*-axis of the mineral crystal structure is aligned parallel to the long axis of the collagen.[94] Owing to its 1D structure, nanocellulose is a favorable building block to mimic these natural aligned mineralized architectures. Nanocellulose could form highly-ordered aligned structures using shear forces produced by wet-spinning, cold-drawing and blade coating. Larger shear forces usually cause higher alignment order. For example, Iwamoto *et al.*, showed that the wet spinning rate of CNFs increased from 0.1 to 100 m min^{-1} leading to the orientation index enhanced from 0.44 to 0.54, finally producing aligned cellulose fibers with a high strength of 321 MPa and modulus of 23.6 GPa.[95] Söderberg *et al.*, developed a flow-assisted organization technique, which allows the assembly of CNFs into macroscale fibers with nearly perfect unidirectional alignment.[96] These highly aligned structures are ideal templates for the incorporation of functional mineral NPs.[97] Zhu *et al.*, used water soluble precursor minerals to infiltrate the aligned CNF network, obtaining an aligned HAp nanocrystal mineralized CNF network that is strikingly similar to bone.[98,99]

Furthermore, progress has been achieved to assemble 1D ultralong HAp nanowires and soft polymers into highly aligned structures with good mechanical properties. Tooth enamel is the hardest tissue in the human body and it exhibits excellent resistance to vibrational damage due to parallelly oriented nanoscale HAp nanowires interconnected by a confined biomolecule matrix in the early tooth development stage. To mimic this enamel structure, excellent alignment of HAp nanowires in the poly(vinyl alcohol) (PVA) matrix has been realized thorough ice-templating and subsequent compression.[100] Due to the versatility of these assembly techniques, the co-assembly of 1D mineral nanowires with nanocellulose is another promising strategy to produce aligned hybrid structures although there are only limited studies reporting this co-assembly. For example, silver nanowires have been co-assembled with bacterial cellulose to produce conductive fibers by wet spinning for pressure and proximity sensing, which could detect and recognize the weak signal of the human voice and pulse waves with high accuracy.[101]

3.2 Two dimensional (2D) layered structures

Nacre is one representative 2D biological structural material involving the coexistence of high strength and notable toughness, as well as brilliant iridescence.[102,103] In a typical nacre nanoarchitecture, numerous hexagonal aragonite platelets with 0.5–1 μm thickness and 10–20 μm width are alternatively stacked with thin biopolymeric layers (5–30 nm thick) of silk protein/chitin (an interlamellar membrane) to form a 2D layered structure.[104] This highly ordered layered structure combined with strong interfacial strength could greatly facilitate the pull-out and bridging between the mineral platelets, the shearing resistance caused by viscoelastic biopolymer glue and tablet interlocking.[105,106] These hierarchical fracture mechanisms synergistically result in nacre being a tough and hard biological material, although its building blocks consist of only brittle minerals and weak polymers.[107] Additionally, this 2D layered morphology is a photonic structure in the dimension of visible light wavelength that can produce multi-layer light interferences, leading to a view-angle-dependent iridescence or the metallic mirror-like luster of nacre.[7,103] Such an outstanding combination of mechanical and photonic properties of nacre provides tremendous inspiration to construct corresponding biomimetic layered structures. To date, efforts to mimic the layered structure using cellulose can be mainly classified into two categories: self-assembly of cellulose and 2D nanomaterials, and layer-by-layer (LbL) growth.

3.2.1 Self-assembly. Owing to the easy operation and scale-up, the combination of cellulose and 2D nanoplates has been frequently assembled into the ''brick and mortar'' layered structure by evaporation induced self-assembly or vacuum assisted filtration. In biomimetic nanostructures, cellulose often acts as the soft biopolymeric glue to enhance the interfacial strength, while mineral plates work as the hard and impact resistant components. Plate-like nanoclays (*e.g.*, montmorillonite, MTM) are one of the most used 2D mineral platelets to fabricate the layered nanocomposites due to their low-cost, abundant sources and water solubility. The selection of cellulose to build this layer structure varies from molecular cellulose to nanocellulose. Walther *et al.* reported nacre-mimetic fire barrier coatings with a well-defined layered structure through the self-assembly of CMC and MTM. Benefiting from the strong interfacial hydrogen bonding and hydrophobic effect, CMC quickly absorbs on the MTM nanoplatelets surface to form core/shell nanoplatelets, which can further self-assemble into a well-ordered layered architecture during water evaporation.[108] Besides, nanocellulose has also been widely used to provide additional mechanical enhancement due to its outstanding mechanical properties. For example, Liu *et al.*, prepared transparent, strong, and flexible layered composites with mineral contents up to 60 wt% by vacuum assisted filtration of aminoclays (AC) and carboxylated cellulose nanofibrils (CNF).[109] The strong electrostatic interaction and well-ordered structure enable the composite films with a high strength of 230 MPa and toughness of 20 MJ m^{-3}, which far exceed those of nacre (80–135 MPa, MJ m^{-3}).[11,110] Similarly, these assembly strategies have also been widely adopted in

other studies to assemble cellulose with other types of functional inorganic nanoplates, such as boron nitride, MXene and MoS_2.[89–114]

Conventional nacre-like composites are often simplified as binary composites, which adapt two components to mimic the mineral phases and polymer phase of nacres, respectively. However, nacre should be treated as a ternary composite because its organic phase consists of chitin nanofibers and silk-like proteins.[115] The alternate stacking of aragonite platelets and nanofibrillar chitin network layers is glued by a soft protein adhesive, providing hierarchical interfacial strength for efficient load transfer.[116,117] To mimic this ternary structure, the third soft polymeric components were usually added to the above binary combination. For example, Wang *et al.*, combined PVA with the clay platelet/CNF to construct strong and transparent artificial nacre based on an evaporation-induced self-assembly technique (Fig. 4(a)).[116] The strong interfacial strength combined with the synergistic toughening effect equips artificial nacre with an excellent balance of strength and toughness, superior to natural nacre and other conventional layered clay/polymer binary composites.[118–120]

3.2.2 Layer-by-layer growth. LbL growth is another popular approach to manufacture nacre-like multilayered thin membranes and coatings. This technique alternatively deposits the desired components on substrates through various non-covalent interfacial interactions, such as hydrogen bonding, electrostatic interactions, and hydrophobic interactions. Consequently, the as-prepared thin film is capable of precisely controlling the thickness of each layer and the distribution/content of components down to the molecular layer level. Another advantage of the LbL technique is its versatility to be applied on various substrates with a rough/smooth surface or different size/geometry, such as flat wafers, flexible films, fibers, particles, and textiles, *via* spin-coating, spray-coating,

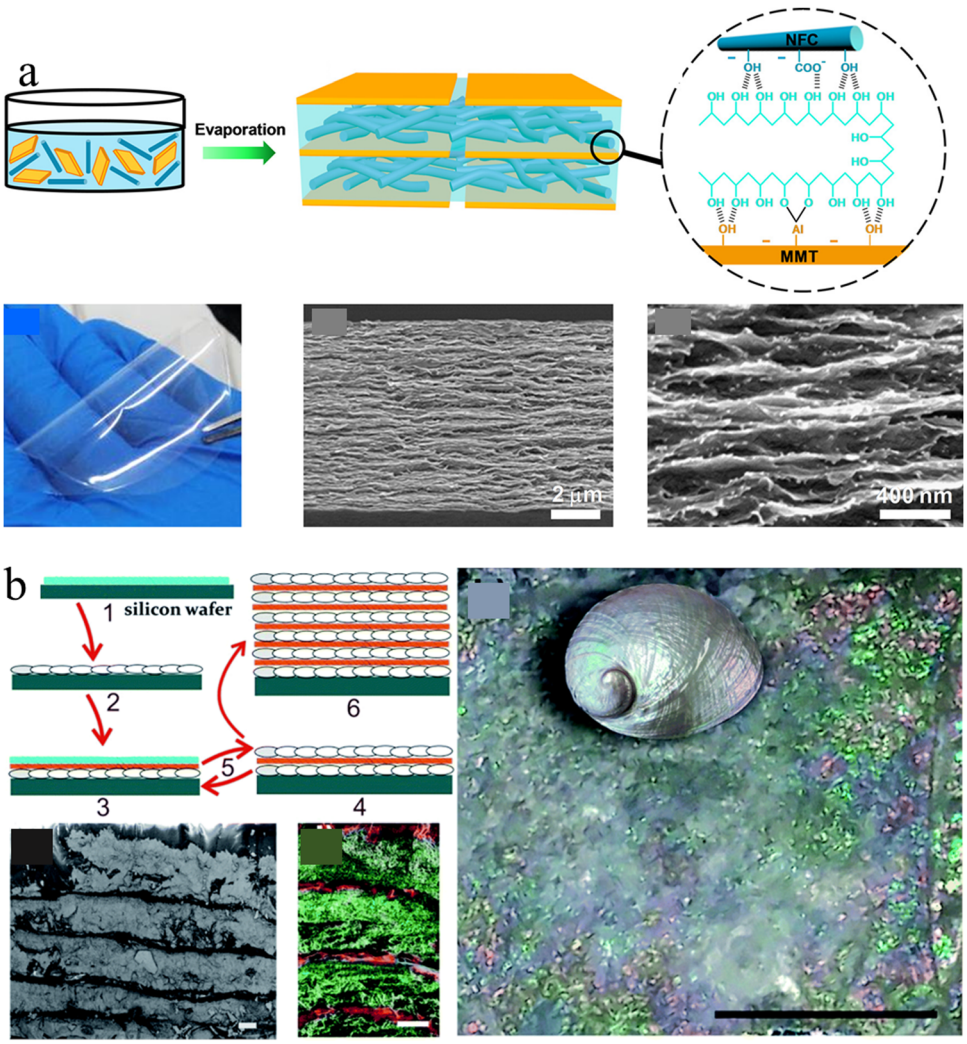

Fig. 4 (a) Schematic illustration of a transparent artificial nacre film prepared from MMT platelets, CNF, and PVA by evaporation induced assembly, and the photo and cross-section SEM images of the corresponding film. Reprinted from ref. 116 with permission of the American Chemical Society, copyright 2014. (b) Schematic of the preparation protocol for the nacre-like material by the layer-by-layer deposition of nanocellulose and calcium carbonate, which exhibits a uniform layered structure and brilliant structural color like nacre. Reprinted from ref. 122 with permission from the Royal Society of Chemistry, copyright 2017.

and immersive/dip-coating.[121] For instance, Farhadi-Khouzani *et al.*, sequentially *in situ* grew a $CaCO_3$ layer onto the pre-deposited nanocellulose layer to produce the multilayered structure (Fig. 4(b)).[122] Due to the rich surface chemistry of nanocellulose, the $CaCO_3$ precursors have good compatibility with the nanocellulose layer, enabling the mineralization of a uniform and tunable $CaCO_3$ layer. The resulting layered composites not only exhibit good stiffness, but also display an iridescent appearance similar to that of nacre because of the uniform layered order at visible light wavelength. This structural color is extremely difficult to achieve using conventional self-assembly techniques of cellulose and nanoplates. In another example, brilliant structural color from Bragg stacks of CNCs/SiO_2 layers and polyethylenimine/vermiculite nanoclay (PEI/nanoclay) layers has been generated by a technique using alternative dip-coating.[123] In this multilayer organization, CNCs/SiO_2 layers possess a refractive index of 1.42 and thickness of 288 nm, while PEI/nanoclay layers have a refractive index of 1.65 with a thickness of 90 nm. This large contrast of refractive index between neighboring layers combined with the submicron interspace enable the fabricated systems to exhibit a very similar optical behavior to a beetle, selectively reflecting the desired color in a narrow band and displaying brilliant iridescence.

3.3 Three dimensional (3D) hierarchical architectures

Nature usually builds 3D structurally ordered and environmentally adaptive mineralized composite materials to survive in harsh environments, such as porous and twisted plywood structures, which are more complex than the simplified 1D and 2D structural motifs discussed above. These complex 3D architectures are primarily responsible for the excellent mechanical properties and multifunctionality of these hybrid materials. Porous biomineralized materials, such as the honeycomb-like structure of highly mineralized cuttlebone, typically have a light-weight feature as well as better crush performance and specific energy absorption performance that is comparable to metallic foams.[124] The twisted plywood structure of the dactyl club of mantis shrimps has a bicontinuous structure with hydroxyapatite ($\sim$88 vol%) integrated in an organic matrix. This special interpenetrated 3D structure provides an unusual combination of stiffness and damping.[125] Thus, mimicking these the 3D architectures is remarkable as it presents new opportunities to construct high-performance synthetic materials.

3.3.1 3D printing. 3D printing is an attractive technique that is capable of sufficiently controlling the 3D morphological organization of cellulose materials at the multiscale according to the on-demand design, offering an attractive pathway for fabricating sustainable structures. These pre-designed ordered structures can work as customized scaffolds to guide the mineralization pathway to form microstructures with ordered orientations. The rich surface chemistry of cellulose and its derivatives enables them to be promising for application in 3D printing bio-inks. Recently, numerous efforts have been dedicated to developing cellulose based biocompatible ink formulations. Due to the strong intra- and inter-molecular hydrogen bonds, cellulose cannot be melt-processed and is insoluble in water and in common organic solvents. Only a few solvent systems have been developed to dissolve cellulose, but most of them suffer from high toxicity, high-cost and are environmentally harmful, limiting their biomedical applications. Ionic liquids (ILs) are promising "green" solvents for cellulose, which are recyclable, chemically and thermally stable and non-volatile. Markstedt *et al.* reported the 3D printing of a tailored cellulose structure using IL dissolved cellulose inks and following water coagulation.[126] Compared with the cellulose solution, cellulose ethers such as EC, HPC and CMC are more frequently used in 3D printing inks due to their good water-solubility. These cellulose ethers could work as viscosity modifiers and matrixes due to their viscosity thickening capability and thixotropic rheology.[127]

Nanocellulose is a highly attractive biodegradable reinforcing nanofiller for strong composites due to its ultrahigh stiffness and strength, high aspect ratio and abundant functional groups. The outstanding mechanical robustness of nanocellulose also could greatly increase the mechanical integrity of the 3D printed products. Additionally, nanocellulose also has strong shear thinning properties that are critical for 3D printing. Thus, nanocellulose has often been added into other biopolymer matrixes to prepare the bio-inks. Markstedt *et al.* combined the shear thinning properties of CNF and the fast cross-linking ability of alginate to prepare bio-inks for the 3D bio-printing of structures of the human ear and sheep meniscus.[128] Usually, the strong shearing force during 3D printing can induce the alignment of nanocellulose along the printing nozzle. This alignment of nanocellulose not only greatly enhances the mechanical properties of the as-prepared products but also provides additional anisotropic functionalities. For example, Gladman *et al.*, printed composite hydrogel architectures with the alignment of CNFs along pre-designed printing pathways. The resulting swelling anisotropies in water lead to shape transformations that occur on the order of minutes.[129] Additionally, nanocellulose could be used as an individual building block to construct the 3D structures. Nanocellulose readily forms a hydrogel at high concentration due to chemical interactions of abundant hydroxyl groups and the physical fibril entanglement. The high zero shear viscosity and shear thinning features make nanocellulose hydrogels an ideal bioink for 3D printing of various aligned structures.[130–132]

The incorporation of mineral components into the 3D printed structures could be achieved through either pre-mixing with cellulose bioinks or the post templated guided growth. For example, HAp NPs are frequently added into the cellulose based bioinks to 3D print plausible scaffolds for bone tissue engineering.[133–135] The addition of nano-sized HAp not only can enhance the mechanical properties of the scaffolds, but also provides the bioactivity and *vice-versa* to mimic the natural bone compositions.[136,137] However, it is worth noting that the direct mixing of HAp powder with cellulose bio-inks usually results in a lack of homogeneity and restricted bioactivity. Therefore, *in situ* mineralization is another effective method to construct hierarchical mineralized composites.[138,139] This strategy highly relies on the pre-printed cellulose scaffolds,

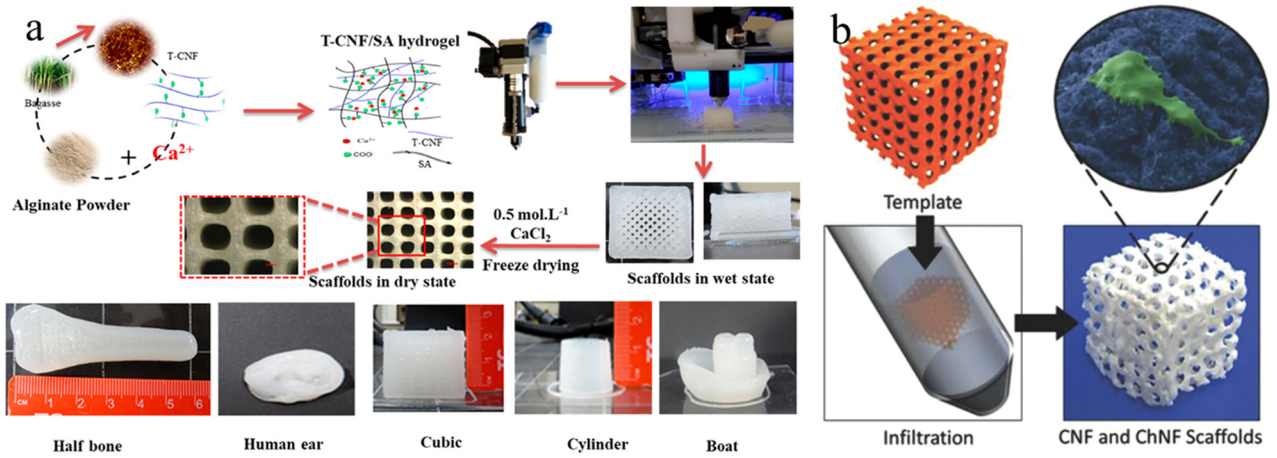

Fig. 5 (a) Fabrication process for 3D printing CNF/alginate scaffolds and different printed scaffold forms. Reprinted from ref. 140 with permission of the American Chemical Society, copyright 2018. (b) The fabrication strategy of CNF/chitin hydrogel inverse scaffolds from 3D printed templates. Reprinted from ref. 141 with permission of Wiley, copyright 2015.

where the surface groups of scaffolds serve as nucleation sites, and the porous scaffolds guide the mineral growth, eventually leading to biomimetic mineralized composites with predesigned microstructures.[138] For instance, Abouzeid *et al.*, reported the 3D printing of a CNF/alginate scaffold using CNF/alginate hydrogel partially crosslinked by calcium ions (Fig. 5(a)).[140] The subsequent full crosslinking of the prepared scaffold could provide the scaffold with good rigidity and long-term stability for the biomimetic mineralization process. As a result, dense HAp successfully grew around the printed scaffolds using simulated body fluid.[140] Moreover, Torres-Rendon *et al.* demonstrated a new reverse templating strategy to construct ordered CNF/chitin hydrogel scaffolds (Fig. 5(b)).[141] In this approach, the pre-designed sacrificial resin templates were fabricated by lithographic 3D printing, which were then infiltrated by the CNF/chitin hydrogel. The removal of resin templates left the CNF/chitin hydrogel with a highly ordered replicated structure for bone tissue engineering.

3.3.2 Ice-templating assembly. Freeze casting is a well-established processing technique to produce porous bulk composites with controlled and complex cellular architectures. This technique often involves freezing water-based (or other solvent) suspensions, followed by sublimation of the solidified solvent phase from the solid to the gas state under vacuum conditions. During the ice growth, building blocks in the slurry are rejected by the moving solidification front, concentrated and entrapped in-between the ice crystals. As a result, porous structures with unidirectional channels in the case of unidirectional freezing can be obtained, where pores are a replica of the solvent crystals.[142] The freeze casting technique is efficient, low-cost, and environmentally friendly, which can be extended to a wide range of building block combinations, including polymers, nanoparticles, nanosheets, and ceramics.[143] In a typical freezing cast process, the pre-degassed building block slurry with the desired viscosity is filled into a mold, which could be further placed on a cold cooper plate, which undergoes isotropic or anisotropic cooling to induce homogeneous or directional solidification. By controlling the temperature gradient in the slurry, the ice crystal directional growth could be readily manipulated. The resulting porous materials exhibit highly ordered directional pores, such as honeycomb pores and lamellar structures.[144]

This strategy was widely used for nanocellulose dispersions or with additional mineral NPs to produce anisotropic aerogels.[145–151] Munier *et al.*, reported that the unidirectional freezing of nanocellulose dispersions can lead to the good alignment of nanocellulose along the freezing direction.[152] The resulting nanocellulose network is even sufficiently strong to resist melting. Chau *et al.*, showed that nanocellulose aerogels with fibrillar, columnar, or lamellar structures can be constructed through the control of the composition of the nanocellulose dispersion and the freeze-casting temperature.[151] Additionally, mineral NPs have often been added into the cellulose matrix to provide mechanical integrity and functionalities.[145,153–155] For example, boron nitride nanosheets have been combined with an anisotropic aerogel to enhance the thermal management properties, such as high conductivity, thermal storage and flame resistance.[156,157] In a recent work, Zhang *et al.*, developed an interfacial engineering strategy to fabricate a mineralized bacterial cellulose aerogel with high compressibility and multifunctionality (Fig. 6).[158] In this approach, nanocellulose with methyltrimethoxysilane (MTMS) was assembled into an anisotropic aerogel using the directional freezing technique, and subsequently polymethylsilsesquioxane (PMSQ) was mineralized as a coating on the bacterial cellulose networks to provide additional interfacial strength. As a result, this mineralized aerogel can achieve low density, mechanical robustness, ultrahigh compressibility, and superhydrophobicity.

3.3.3 Self-assembly of chiral nematic liquid crystal structures. Chiral nematic structures, also called twisted plywood structures or Bouligand structures, are commonly found in the animal and plant kingdom. This structure not only has hierarchical toughening mechanisms to enhance the mechanical properties, but also can precisely control the light–matter interaction for producing the desired photonic properties, such

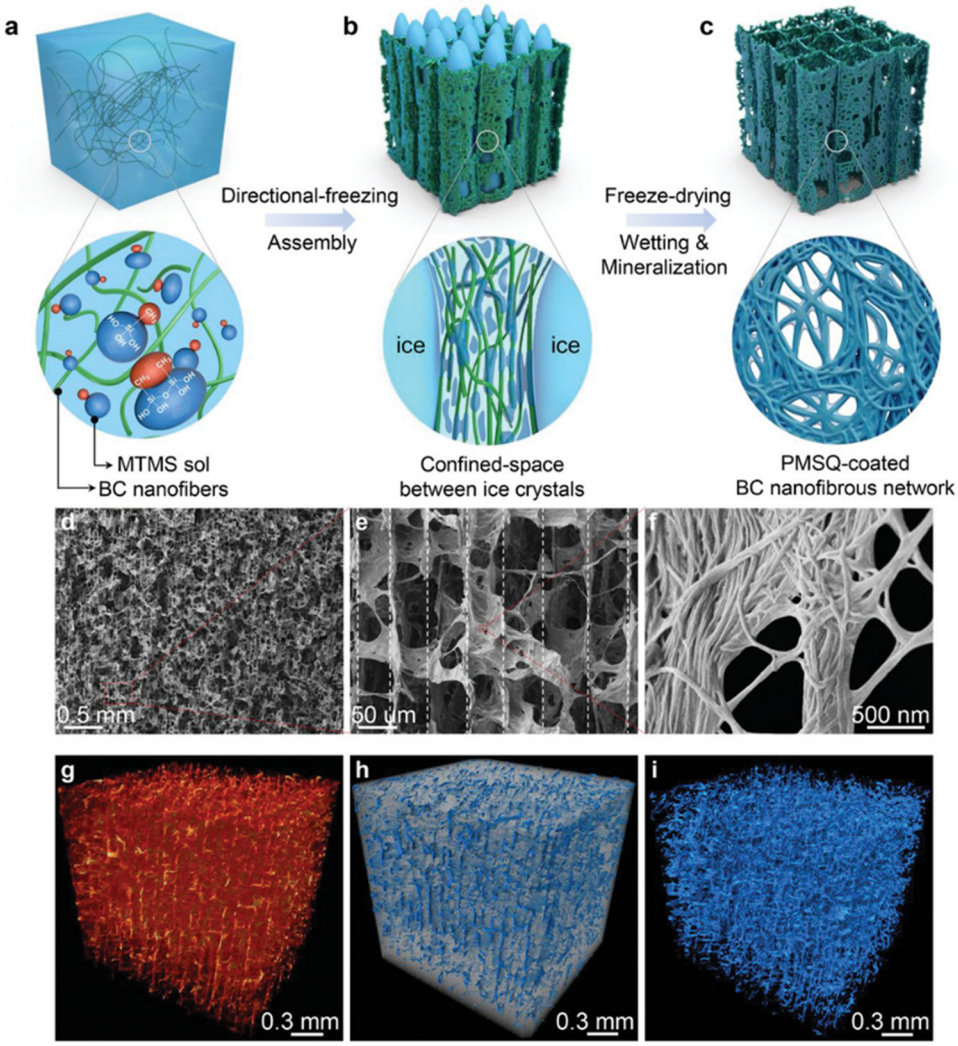

Fig. 6 (a)–(c) The schematic illustration of the synthesis of anisotropic BC–PMSQ aerogel. (d)–(f) SEM images of the microscopic structure of the BC–PMSQ aerogel at different magnifications. (g)–(i) Reconstructed 3D micro-CT image of the representative BC–PMSQ hybrid aerogel, showing the two distinctive regions of the macropores and solid framework. Reprinted from ref. 158 with permission of Wiley, copyright 2021.

as structural color and circular dichroism (CD). Learning from nature's engineering principles is a promising approach to construct high performance chiral materials with efficient light management properties, but recreating their chiral architectures, especially at the macroscopic or bulk scale, is challenging from both fundamental scientific and engineering perspectives.[159] To date, very few examples have been reported to successfully mimic the twisted plywood structure *via* 3D printing,[160] brush induced self-assembly[161] and magnetic-field-assisted slip-casting techniques[162] because of the difficulty in balancing good organization of the hierarchical structure and efficiency. As a result, with these synthetic materials it is difficult to achieve the mechanical enhancement and iridescent structural color that is observed in living organisms.

Rod-like CNCs can form chiral nematic liquid crystal phases, which are similar to the natural Bouligand structure, in concentrated aqueous dispersions controlled by solution concentration.[163] Liquid chiral nematic phases have long-range order with the pitch of helical structures in the range of tens of micrometers. However, the water evaporation causes the chiral pitch to reduce to the submicron range, leading to Bragg's light reflection in the visible spectrum and bright structural colors. This pitch distance can be adjusted by varying the sonication time, temperature, and the addition of salt and soft polymers for regulating the reflectivity.[7,56,163,164] To obtain the bio-inorganic hybrid chiral structure, inorganic NPs usually co-assemble with CNCs into the chiral nematic liquid crystal phase, which is finally preserved in a solid film. To date, various functional NPs, such as gold nanoclusters, metal NPs, quantum dots and nanorods, have been added into the chiral CNC host matrix to construct functional chiral materials.[165–171] In a recent study, Kang *et al.*, used semiconducting quantum nanorods (QNRs) to co-assemble with CNC to prepare the chiral composites with a combination of tunable iridescence and active photoluminescence.[165] The similar geometry and size between QNR and CNC allow the seamless co-assembly of highly ordered chiral nematic structures with

unusually large photoluminescent asymmetry. Additional incorporation of elastic polymers further enhances the stretchability of the composites with stress induced dynamic photonic properties.

Moreover, this highly-ordered chiral cellulose nanostructure with confined interspace is also an ideal template for biomineralization with multiscale length hierarchy. Shopsowitz *et al.*, developed photonic mesoporous silica films using the CNC chiral nematic liquid crystal structure as a biotemplate. They co-assembled silica precursors with CNC to form a chiral nematic phase, and the silica precursors can be hydrolyzed into silica by the acidic nature of the CNCs. With pyrolysis treatment, the CNC template can be removed to leave the mesoporous inorganic silica films in the free-standing state. Although the chiral nematic structure has promising toughening mechanisms, the prepared CNC chiral nematic composite films are usually very weak and brittle, which significantly limits their applications. Inspired by the natural molting process of crustaceans to produce a strong dactyl club and exoskeletons, our groups recently developed an artificial molting process to construct strong and tough mineralized CNC composites combined with tunable photonic properties (Fig. 7).[172] The highly ordered chiral nematic structure of soft templates assembled from CNC and polyacrylic acid (PAA) can efficiently regulate the mineralization process of calcium carbonates. A short mineralization time results in a strong and flexible endocuticle-like structure, while prolonged mineralization causes a stiff and hard exo/endocuticle-like biphasic sandwich structure.[172]

3.3.4 Wood-scaffold templating mineralization. Wood has a sophisticated hierarchical porous structure that can be utilized as a bio-scaffold for biomineralization. Numerous cellulose nanofibers with a diameter down to 3 nm highly align in the hemicellulose/lignin matrix to constitute the wood cell walls with high stiffness and strength. To obtain efficient water transport properties and mechanical stability, wood evolved into a unique highly porous unidirectional tubular structure. This structure combines density-different earlywood and latewood, where earlywood consists of axially oriented cells with thin walls and wide lumina to facilitate water transport, while the latewood contains thick-walled cells with narrow lumina for mechanical support.[173] This anisotropic porous structure combined with outstanding mechanical stability and rich surface chemistry makes wood an ideal scaffold to grow mineral NPs for providing additional functionalities.[174] Silanes have been widely adopted to grow silicon on the wood scaffolds due to their large variety of compounds and chemical functionalities. Using a vacuum assisted infiltration technique, silane monomers or oligomers can quickly infiltrate into the wood scaffold and can be subsequently hydrolyzed into SiO_2 NPs to attach to the wood cell wall.[175,176] Magnetic NPs are another good example to integrate magnetic functionality into wood scaffolds. Merk *et al.*, successfully fabricated magnetic wood by *in situ* growth of iron oxide NPs along the directional wood scaffold (Fig. 8(a)).[177] The anisotropic organization of wood scaffolds can provide the magnetic functionalities with good anisotropic properties, thus allowing the directional manipulation of the magnetic wood using a magnetic field. Similarly, $CaCO_3$ has also been *in situ* grown inside the wood scaffolds to provide the wood with enhanced fire retardancy.[178]

However, these wood–mineral composites usually face issues of non-uniform mineral distribution and a small amount of mineral loading due to the hierarchical pore size and the closed pores caused by the sample preparation. To increase the porosity of the wood scaffold, delignification treatment has

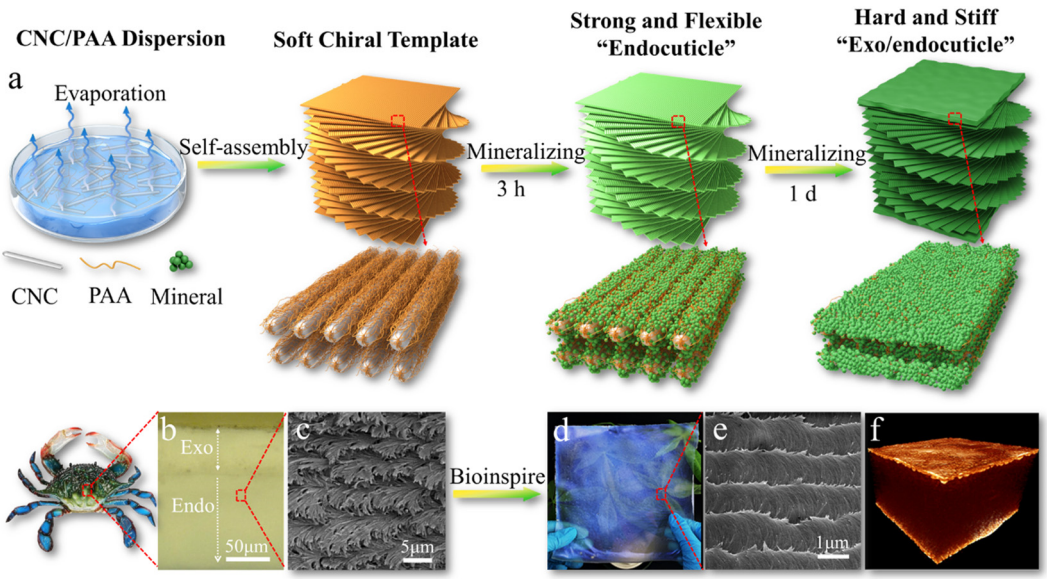

Fig. 7 (a) Schematic illustration of mineralized CNC chiral composites with strong mechanical properties and bio-photonics; (b) the exo/endocuticle structure of crab exoskeletons; (c) the chiral structure of crab endocuticles. (d) A photo and (e) the biomimetic chiral structure of a large-area biomimetic iridescent film mineralized for 3 h. (f) X-ray tomography 3D image of the sandwiched structure of the biomimetic film mineralized for 1 d. Reprinted from ref. 172 with permission of Wiley, copyright 2021.

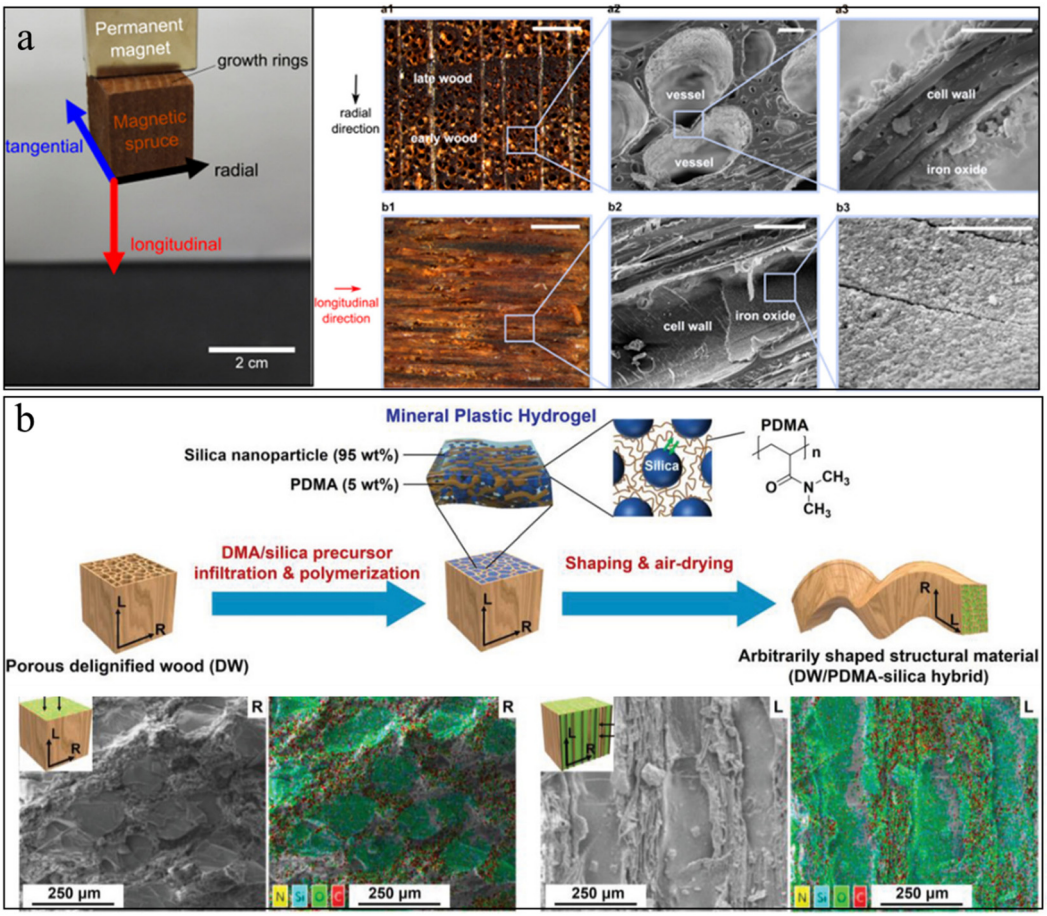

Fig. 8 (a) Photo of magnetic wood by *in situ* growth of magnetic NPs inside the wood, and the corresponding SEM image of magnetic NPs distribution inside the wood. Reprinted from ref. 177 with permission of the American Chemical Society, copyright 2014. (b) Schematic illustration of wood–inorganic hybrid structural materials with the strategy of mineral plastic hydrogels. The corresponding SEM images show that the minerals filled the wood pores. Reprinted from ref. 182 with permission from Wiley, copyright 2020.

often been applied to the wood. This treatment could partially or fully remove the lignin from the wood scaffold, although it will also reduce the mechanical properties.[179] Additional polymers can infiltrate into these delignified wood scaffolds to work as functional glues to enhance the mechanical properties, as well as to act as nucleation agents to regulate the uniform mineral growth.[180,181] Zhang *et al.*, prepared a mineral plastic hydrogel by infiltrating poly(*N*,*N*-dimethylacrylamide)/silica into a porous delignified wood scaffold (Fig. 8(b)).[182] The as-prepared hydrogel exhibits good hydroplastic properties that allow manipulation of the hydrogel into arbitrary shapes. These designed shapes can be preserved after drying and good strength and toughness were obtained. In another example, Wang *et al.*, infiltrated biocompatible alginate hydrogels into the microchannels of a delignified wood scaffold followed by *in situ* mineralization of HAp nanocrystals.[183] The strong interfacial strength and the combination of HAp nanofillers with aligned cellulose scaffolds provide the mineralized composites with a high strength and modulus that are three orders of magnitude higher than those of conventional alginate hydrogels.

Besides, the study of mineralized cellulose mechanisms is a research hotspot. Generally, there are many techniques to explore the underlying mechanism of mineralized nanocellulose materials, such as small-angle scattering (SAS), quartz crystal microbalance with dissipation monitoring (QCM-D), cryogenic electron microscopy, tomography and computer simulations of materials. Computer simulations are a feasible and rapid way to study the reactions and structures of mineralized nanocellulose. By comparing the computational results and experimental data, researchers can predict hypothetical model structures and properties.[184] However, simulations are suitable for specific length scales and it is hard to examine the integration of mineralized cellulose with complex structures like hierarchies.[185] The common simulations methods include Ab inito electronic structures simulations, peridynamics simulations, phase field models simulations, the finite element method (FEM), all-atom MD stimulations, reactive molecular dynamics (MD) simulations, atomistic MD simulations, and coarse-grained (CG) simulations.[186] All these simulations could be utilized solely or in combination to predict the structure and function across different length scales.

4. Biomedical applications

Bioinspired mineralization is a process in which researchers mimic biomineralization and utilize a biological matrix as a template to regulate the nucleation, orientation, growth, and self-assembly of inorganic minerals.[187] This revolutionary approach exhibits tremendous potential to produce extraordinary biomaterials by integrating organic–inorganic composites with micro- or nano-scale replication of hierarchical natural structures (*e.g.*, bone, dentin, and enamel), defining novel properties with coating biomolecules or chemicals (*e.g.*, soft tissue engineering, anticancer, antibacterial, and drug delivery).

Cellulose is a nature-derived polymer with excellent mechanical properties, fine tunability in functional groups modification and morphology, green properties (*e.g.*, record biocompatibility, nontoxicity, and biodegradability), abundance, and accessibility.[188] Cellulose, as a "multi-use mucilage," is introduced to bioinspired mineralization and envisioned for the most promising future directions in the field of biomedical applications.[189–193] Cellulose related materials exhibit extraordinary properties with bioinspired mineralization, especially in terms of physicochemical, mechanical, biodegradability and *in vitro*/*in vivo* properties along with non-mineralized cellulose (Table 2). However, there are only a few reported studies investigating the mineralized cellulose-based scaffolds for

Table 2 Details of the properties of non-mineralized cellulose and mineralized cellulose

Properties/materials		Non-mineralized cellulose	Mineralized cellulose (synergistic type)	Ref.
Hydrogel		CNF composite hydrogel	CNF composite hydrogel with bioactive glass	199
Physicochemical	Viscosity (Pa s)	176 ± 16	838 ± 123	
	Spreading ratio	0.78 ± 0.11	0.89 ± 0.18	
Biological function	Ion release	(—)	Release of B, Si, Sr, Mg, Ca, and P	
	In vitro cell biology	Good viability and proliferation ability in Saos-2 cells and hBMSCs	Slight decreased viability and proliferation ability, but higher osteogenic ability in Saos-2 cells and hBMSCs	
Hydrogel		Cellulose hydrogels	Cellulose/HAP nanocomposite hydrogels	200
Physicochemical	Recyclability	96.58%	78.60%	
Mechanical	Young's modulus (kPa)	69	333	
	Compressive stress (kPa)	100	401–570	
Cryogel		CNC cryogel	Mineralized CNC cryogel with SBF	201
Physicochemical	Weight loss of the samples immersed in PBS for 21 days	25.3 ± 2.0%	~47.9 ± 4.4%	
Mechanical	Young's modulus (kPa)	4.1 ± 0.6	~3.4 ± 0.3	
Biological function	Cell viability of human adipose-derived stem cells (hASCs)	>90% lives three days after seeding		
	Metabolic activity and cell proliferation		Better	
	Osteogenesis ability of hASCs	(—)	Higher ALP activity and increased gene expression of RUNX2, COL1A1, BMP-2, DKK-1, and PDPN	
	Release of PDGF and VEGF (pg ml^{-1})	50 for PDGF 40 for VEGF	30 for PDGF 25 for VEGF	
Bacterial cellulose		Aligned-BC	Mineralized aBC *in situ*	
Physicochemical	Thermal stability	225–350 °C	350–480 °C	
	Weight loss (%) between 150 and 450 °C	90.37 ± 2.59	51.68 ± 2.06	202 and 203
	T_{max} (°C) at decomposition	375.9 ± 3.2	351.4 ± 2.5	
	Surface morphology	Less dense arrangement of fibrils	More dense arrangement of fibrils	
Mechanical	Elastic modulus (Gpa)	5	10	
	Hardness (Gpa)	0.1	0.6	
Degradation	*In vitro* degradation with cellulosic enzyme	Degraded in 5 days	Slower degradation speed	
Biological function	*In vitro* cell biology		Better attachment and proliferation in the two-day cultivation of MC3T3-E1	
		Cellulose nanofibers	Mineralized cellulose nanofibers with SBF	204
Physicochemical	Thickness (mm)	0.092 ± 0.004	0.149 ± 0.013	
	Surface pH	7.0 ± 0.23	6.6 ± 0.091	
Mechanical	Tensile strength (MPa)	21.25 ± 1.41	26.25 ± 2.50	
	Strain at maximum load (%)	16.33 ± 3.053	24.97 ± 2.95	
	Modulus of elasticity (MPa)	687.5 ± 102.1	815.9 ± 93.9	
Biological function	Ion release		Release of Ca, P and F	
	Ability to remineralize the demineralized teeth *in vitro*		Increase the Vickers hardness number from 41.2 ± 0.09 to 137.7 ± 0.1	

medical related tissue engineering so far. Thus, much of the work on this subject needs further effort. In this part, we summarize the biomedical applications of cellulose and its derivates *via* biomimetic mineralization. However, a more detailed insight into this topic is provided in dedicated reviews.[20,25,194–198]

4.1 Hard tissue engineering

Biomineralization in nature primarily involves the mineralization process of bone, teeth, and shells. Bone, a hierarchical–architecture nanocomposite material, is mainly made of inorganic hydroxyapatite nanocrystallites and a collagen-rich organic matrix.[205,206] Bone can be considered as the self-assembly of insoluble collagen fibrils as a structural template mineralized with nanoscopic apatite platelets, thus exhibiting unique mechanical properties.[206,207] Nanocellulose is promising as a base organic matrix for biomineralization, which applies to the tissue engineering of bone, dentin, and enamel repair since the multi-scale hierarchical anisotropic structure has been the greatest advantage for wood.

4.1.1 Wood as a template for bone regeneration. Wood and bone both have ultrastrong and stiff mechanical properties because of their hierarchical anisotropic structure.[208] Inspired by the structure, wood has also been used as a template for porous bioceramic scaffolds of bone substitutes. Simone *et al.* selected cylindrical wood pieces as a model material to make the apatite scaffold (Fig. 9(a)). The apatite scaffold ultimately exhibited a similar nanostructure to osteons typical of compact bone.[209] Wang *et al.* fabricated highly anisotropic, hydrophilic, and osteoconductive hydrogel composites *via* impregnation of biocompatible hydrogels into the microchannels of delignified wood followed by *in situ* mineralization of HAp nanocrystals. They chose natural pinewood as the model to make aligned cellulose fibril skeletons and selected sodium alginate (SA) hydrogel with calcium ions to infiltrate into the skeletons, thus obtaining an *in situ* mineralized artificial bone substitute. The wood-original composites show a similar elastic modulus to natural compact bone. In this respect, this biomaterial can be a promising candidate for load-bearing bone repair. Furthermore, the researchers demonstrated that the wood-original composites

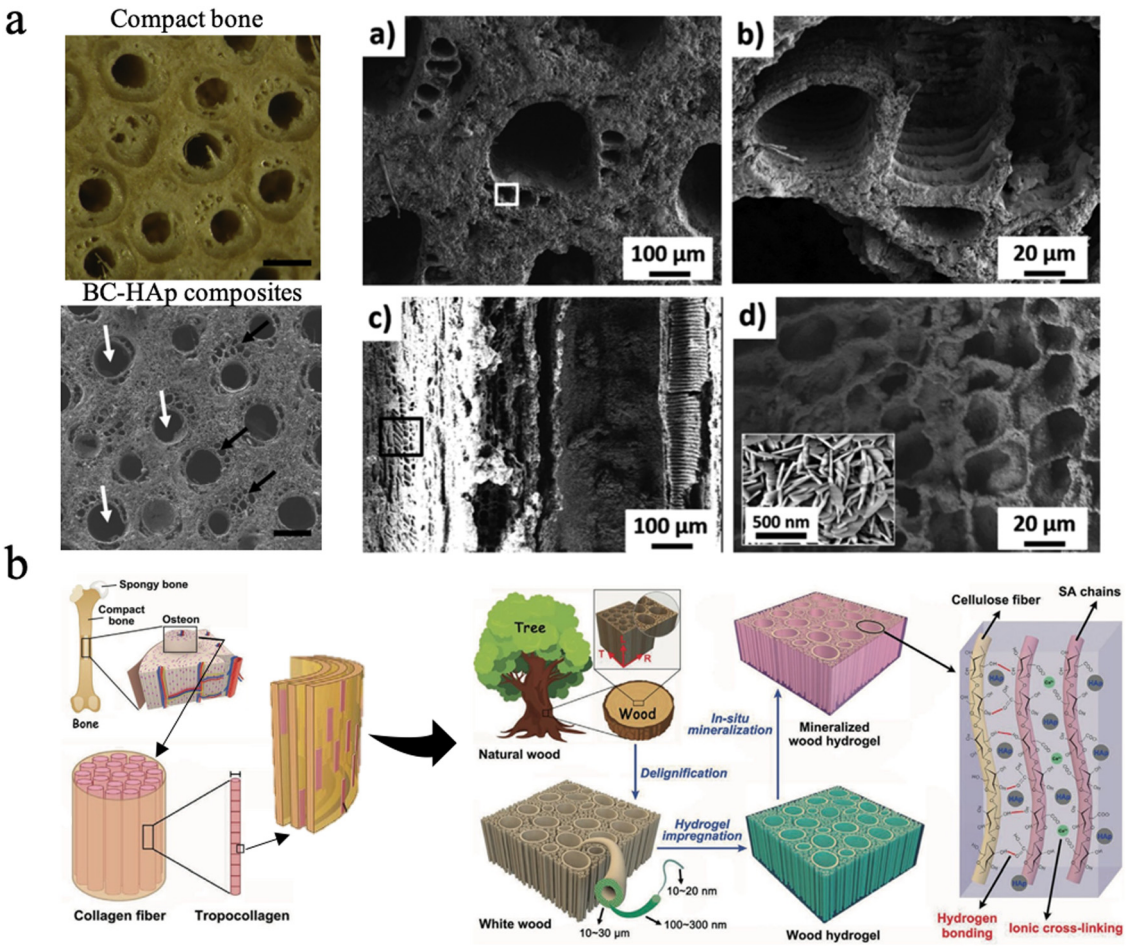

Fig. 9 (a) The SEM picture of BC–Hap composites and the material microstructure at multiple scales, similar to the osteon structure. Reproduced from ref. 209 with permission of Elsevier, Copyright 2020. (b) Design strategy, fabrication and microscopic structure of the mineralized wood hydrogel composite, which is bioinspired by the hierarchical structure of natural bone. Reproduced from ref. 210 with permission of Wiley, Copyright 2021.

induce new bone formation and facilitate osteointegration. However, they also highlighted some limitations of the wood-original composites: large-scale production, lack of cellulase in the human body, and the precious control of uniform porosity were the difficulties that are needed to be solved (Fig. 9(b)).[210]

4.1.2 Biomineralized BC for bone repair. Notably, BC scaffolds have been proven to be an ideal bone regeneration candidate due to their outstanding properties, incredibly compounded with other components. Hu *et al.* prepared bioabsorbable BC composites by immersing BC in simulated body fluids (SBF) followed by cellulase enzyme incorporation.[203] They revealed an improved approach to disperse Hap nanopowder in SBF in order to enhance the total amount of calcium phosphate (CP). Mouse osteoblasts demonstrated good biocompatibility of the BC composites because of the incorporation of cellulosic enzymes.[203]

Liu *et al.* designed a nanocellulose-reinforced hybrid membrane by assembling ultralong Hap nanobelts in a BC hydrogel.[211] This hybrid membrane was proven to promote rapid new bone growth and the formation of blood capillaries, and nerve regeneration.[211] Moreover, Paul *et al.* also mineralized a BC scaffold with HAp for bone healing applications in simulated body fluid. MSCs showed good adhesion and differentiation on mineralized BC with the results of alkaline phosphatase gene expression.[202,212]

The mineralization of cellulose or BC scaffolds improved their mechanical properties and impeded their applicability in hard tissue regeneration. It is vital that the mechanical strength of bone substitute scaffolds should match that of the surrounding bone tissue to prevent the occurrence of some clinical problems like stress shielding.[193] Cortical bone has a modulus strength ranging from 3 to 17 GPa while cancellous bone has a modulus of 0.44 GPa, since bone strength changes extensively with age as well as the type of bone. In terms of tensile strength, cortical bone shows a tensile strength from 33 to 193 MPa and cancellous bone of approximately 6.8 MPa.[213] Cheng *et al.* mineralized aligned BC through *in situ* mineralization using $CaCl_2$ and K_2HPO_4 solutions to mimic the natural structure of bone. The BC composites exhibited an elastic modulus of 10.91 ± 3.26 GPa and hardness of 0.37 ± 0.18 GPa,[214] which is close to that of cortical bone (Fig. 10(a)).

It is reported that the pore size of scaffolds impacts mesenchymal stem cell growth and adhesion, and neovascularization.[217] The researchers focused on the rational design of pore sizes of cellulose-based scaffolds to balance the mechanical properties and the capability of promoting cell proliferation and differentiation.[215,218] Favi *et al.* designed a microporous BC scaffold with well-defined honeycomb pore arrays inserted into nano-HAp. The BC-HAp scaffolds have a pore size of 300 μm and formed a well-designed port network to mimic the bone microstructure. The porous BC–HAp scaffold showed an ultimate tensile strength of 1.39 ± 0.28 MPa, a strain at break of $23.44 \pm 2.52\%$, and an elastic modulus of 6.73 ± 0.7 MPa. The values for these scaffolds were significantly lower than that of compact human bone, but they are still mechanically suitable for cancellous bone. This study finally proves that the BC–HAp

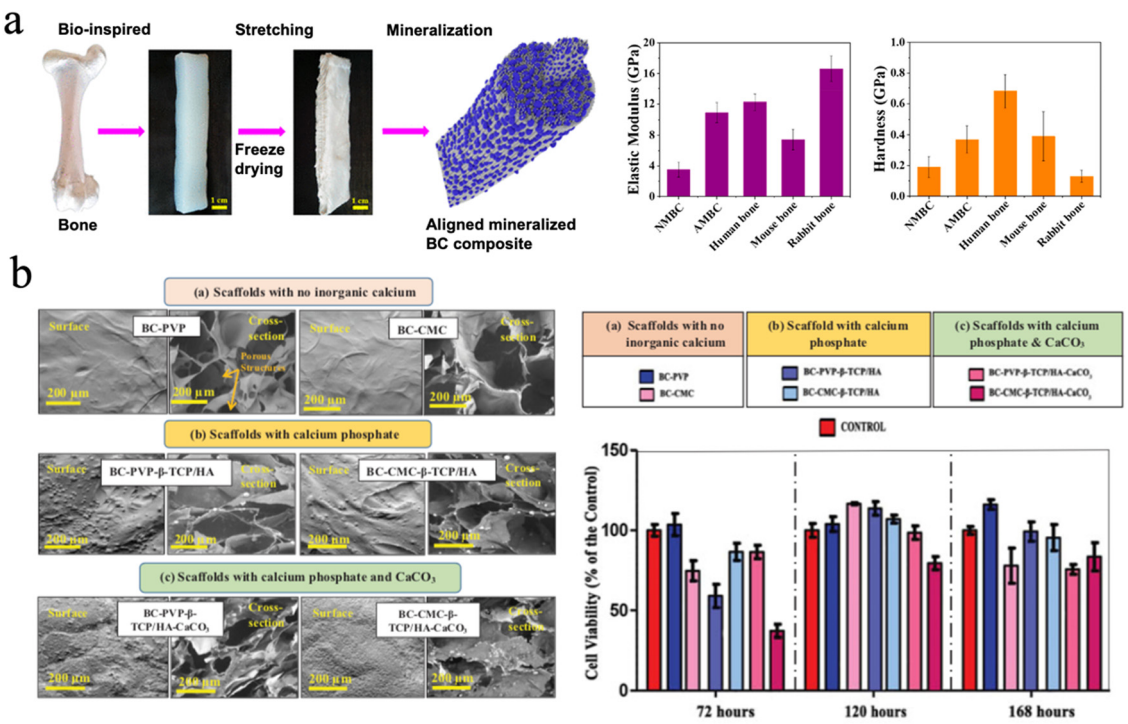

Fig. 10 (a) The aligned mineralized BC composite mimicking the natural structure of bone exhibiting excellent mechanical strength. Reproduced from ref. 214 with permission of the American Chemical Society, copyright 2019. (b) SEM image of BC based hydrogel scaffolds with no inorganic calcium and different calcium fillers, and the cell viability profile of Lep-3 cells on different groups. Reproduced from ref. 223 with permission of Taylor & Francis, Copyright 2018.

scaffolds exhibit good biocompatibility and adhesion for human-derived bone marrow mesenchymal stem cells as compared to native BC scaffolds.[223]

Huang *et al.* fabricated nanostructured macroporous BC scaffolds through an emulsion freeze-drying technique and modified them with gelatin (Gel) *via* the procyanidin (PA) crosslinking technique and HAp coating.[219] They made three other scaffolds named BC, BC/gel, BC/PA/gel. BC scaffolds were prepared with crushed BC, agarose, and deionized water *via* emulsion freeze-drying and BC/gel scaffolds added one more component of gelatin. BC/PA/gel needs one more crosslinking step. The four scaffolds were then compared in terms of their biocompatibility and osteoinductivity. The numbers of macropores and nanopores in BC/gel, BC/PA/gel, and BC/PA/gel/HAp groups all showed a statistically significant increase compared with BC scaffolds, which was proven by the existence of a nanofibrous interconnected network structure. The mechanical results showed the BC/PA/gel/HAp scaffold displayed the highest Young's modulus, maximum load, and compressive strength. The adhesion, viability, proliferation, and osteogenic potential of hBMSCs were investigated after seeding on the different BC scaffolds. The results showed that the BC/PA/gel/HAp scaffold had the highest viability, best adhesion, and the most apparent proliferation and osteogenic differentiation among the four scaffolds. *In vivo* studies also revealed the same tendency of new bone formation in the BC/PA/gel/HAp sample. Therefore, porosity plays a role in promoting cell migration and new tissue formation.[219]

There are many forms of inorganic calcium minerals in nature. They can be simply divided into calcified minerals and noncalcified minerals. There is no doubt that calcium mineral is the main inorganic phase in natural bone.[220] More minerals, such as bioactive glass[221] and biphasic calcium phosphate[222] were chosen to fabricate cellulose-based biomaterials for bone repair. Basu *et al.* focused on the biological efficiency of inorganic calcium-filled BC based hydrogel scaffolds for their future use in bone tissue engineering/bioengineering. They evaluated calcium phosphate, β-tricalcium phosphate (β-TCP) and HAp and calcium carbonate ($CaCO_3$), which were incorporated into BC. All these hydrogel scaffolds facilitated human embryonic fibroblasts (Lep-3) and mouse bone explant cells (BEC) efficient growth and proliferation. However, it was found that BC-based β-TCP/HAp scaffolds show the lowest growth and proliferation of Lep-3 and BEC DNA strands, compared to BC-CMC based β-TCP/HAp scaffolds. BC-based β-TCP/HAp scaffolds facilitated notable cell adhesion and growth and were recommended as the most efficient bone tissue engineering scaffold among the four tested scaffolds (Fig. 10(b)).[216,223]

4.1.3 Other forms of cellulose for bone regeneration. In addition to traditional biomaterials, CNF has been proven to modulate the flow behavior of hydrogels and has a similar structure to extracellular matrices, making it more attractive for 3D bioprinting.[221] Abouzeid *et al.* prepared a three-dimensional printed scaffold with TEMPO-oxidized nanocellulose/alginate hydrogel.[224] The rheological results show that the viscosity recovery for pure alginate hydrogel was only about 16% of the initial value, whereas it was 66% when adding cellulose nanofibrils to alginate. Consequently, TEMPO-oxidized cellulose/alginate hydrogel could maintain its shape and fidelity and prevent the collapse of the filaments to promote new bone formation.[224] Most recently, Guo *et al.* proposed a new strategy *via* a gentle pre-crosslinking to achieve a favorable printability and strong cellulose/bioactive glass hydrogel.[225] The printed cellulose hydrogels exhibited a biomimetic nanofibrous topology as well as remarkable tensile and compressive strength (5.22 and 11.8 MPa). The hydrogels could be printed to mimic the osteochondral structure and *in vivo* rabbit animal experiments demonstrated superior osteochondral defect repair performance (Fig. 11(a)).[225]

Moreover, different sizes of HAp nanoparticles can be chosen to assemble with nanocellulose for different hierarchal tissue regeneration. Zhu *et al.* incorporated CNFs into a double-network (DN) hydrogel scaffold based on covalently cross-linked poly (γ-glutamic acid) (PGA) and ionically cross-linked alginic acid, which was loaded with different sizes of HAp particles, Nano-HAp and Micro-HAp.[226] They found that the Nano-HAp can enhance the compression modulus and osteogenesis, while Micro-HAp was added to promote cartilage matrix deposition. The results showed that the hydrogel exhibits a comparable compression modulus (0.322 MPa) to natural articular cartilage. *In vivo* experiments showed that the bilayer scaffolds with different sizes of HAp design have great osteochondral and bone tissue repair potential (Fig. 11(b)).[226]

Cellulose derivatives are also developed for strengthening properties and are beneficial for bone tissue scaffolding applications. Oliveria *et al.* demonstrate an injectable composite containing CaP glass-ceramic particles, dispersed within a (hydroxypropyl)methyl cellulose (HPMC) matrix, with the capacity to release calcium in a more sustained fashion.[227] The results show that the composite could improve both bone formation and increase angiogenesis *via* a rat bone defect model.[227] CNC with sulfate and phosphate half-ester surface groups were produced by chemical crosslinking and submerged in simulated body fluid solution with a 0.1 M $CaCl_2$ pre-treatment. Sulfated CNC aerogels exhibited good compressive strength and long-term stability in liquid environments and showed their osteoconductive properties with a tremendous increase in bone volume by up to 50% compared to sham sites. Jafari *et al.* reported a novel epichlorohydrin (ECH)-crosslinked hydroxyethyl cellulose (HEC)/soy protein isolate (SPI) porous bi-component scaffold (EHSS) with HAp functionalization for bone defect repair *via* the combination of lyophilization and *in situ* biomimetic mineralization.[228] The scaffold exhibited an interconnected porous structure, which is suitable for MC3T3-E1 cell attachment, proliferation, and growth. The scaffold had a similar Ca/P ratio to natural bone tissue and markedly promoted new bone formation and maturation in *in vivo* experiments.[228] More recently, a novel nitrogen-doped multiwalled carbon nanotube/cellulose/nanoHAp nanocomposite scaffold was synthesized *via* a crosslinking/hydrothermal/freeze-drying method, resulting in layer-by-layer structures with functional and structural properties mimicking natural bone.

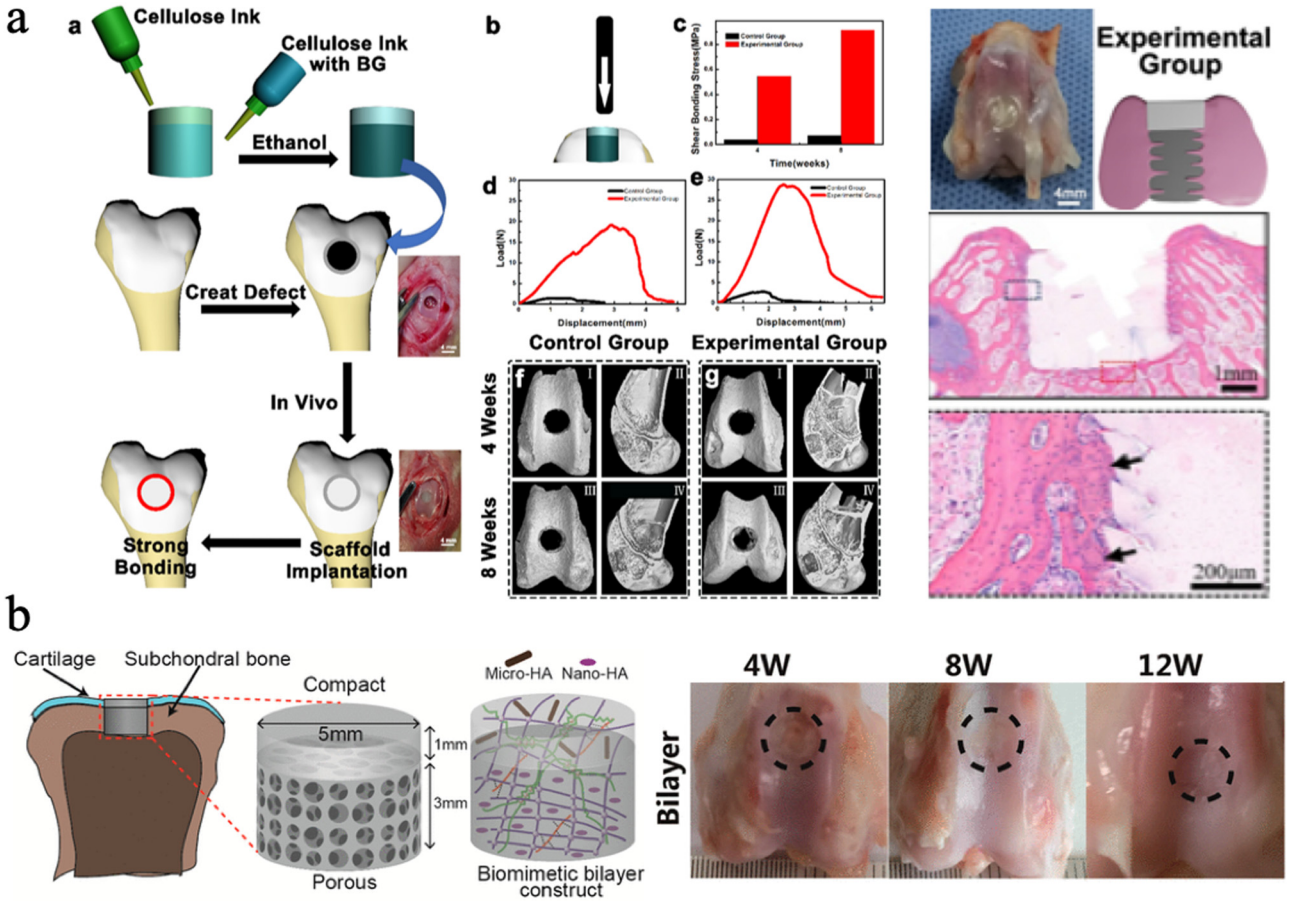

Fig. 11 (a) The push-out test for cellulose ink with bioactive glass, and the histological images with gel plugs implanted into rabbit femurs. Reproduced from ref. 225 with permission of the American Chemical Society, Copyright 2022. (b) Schematic illustration of the bilayer BC based hydrogel, and the macroscopic images of knees repaired with the hydrogel. Reproduced from ref. 226 with permission of the American Chemical Society, copyright 2018.

Importantly, the resulting scaffold has favorable mechanical properties, high porosity, and interconnected architecture, thus providing a suitable microenvironment for bone mesenchymal stem cell (BMSC) proliferation, viability, mineralization, and osteoinduction in *in vitro* cultures. *In vivo* experiments confirmed that the scaffolds not only improved the interface bonding with bone tissue but also accelerated new bone formation and regeneration.[229]

4.1.4 Mineralized cellulose for other hard tissue regeneration. Nanocellulose is also applied to bone implant coatings as a natural polymer in mineralization. Boccaccini *et al.* made an orthopedic implant coating with 45S5 bioactive glass (BG) individually wrapped and interconnected with fibrous CNCs, which was deposited on 316L stainless steel.[230] The coating substantially accelerated the attachment, spreading, proliferation, and differentiation of mouse MC3T3-E1 osteoblast progenitor cells *in vitro* and mineralization of the extracellular matrix deposited by these cells (Fig. 12(a)).[230]

In another field, scientists utilized CNFs to assemble unique structures to mimic other natural hard tissues. These studies expanded the application of CNFs in hard tissue regeneration. Qi *et al.* fabricated highly compacted, aligned CNFs through a nonclassical mineralization process and achieved dentin-like ultrastructures.[232] Zaki *et al.* reported innovative re-mineralizing oral films made from a blend of hydroxyethyl-cellulose (HEC) and CNF, loaded with nepheline fluorapatite glass powder.[204] SEM results revealed that the film has a uniform glass powder particle distribution. They also measured surface hardness by evaluating the films' effect on demineralized enamel micro-hardness. The results showed a significant increase in enamel micro-hardness compared to the demineralized specimen. The cellulose-derived films can be a candidate for remineralization of early demineralized tooth lesions.[204]

Some researchers found that nanocellulose could be organized in a pitch-graded chiral nematic structure to achieve great hardness properties (Fig. 12(b)).[231] They combined assembly of CNCs with genetically engineered protein matrices, which can increase their interfacial strength and mediate nucleation and growth of apatite crystals. By mimicking the impact-resistant dactyl club of the stomatopod, scientists successfully produced this multi-phase nanocomposite with a CNC-based apatite. The resulting bioinspired composite exhibits a graded microstructure with a correlated mechanical gradient that closely resembles those observed in natural

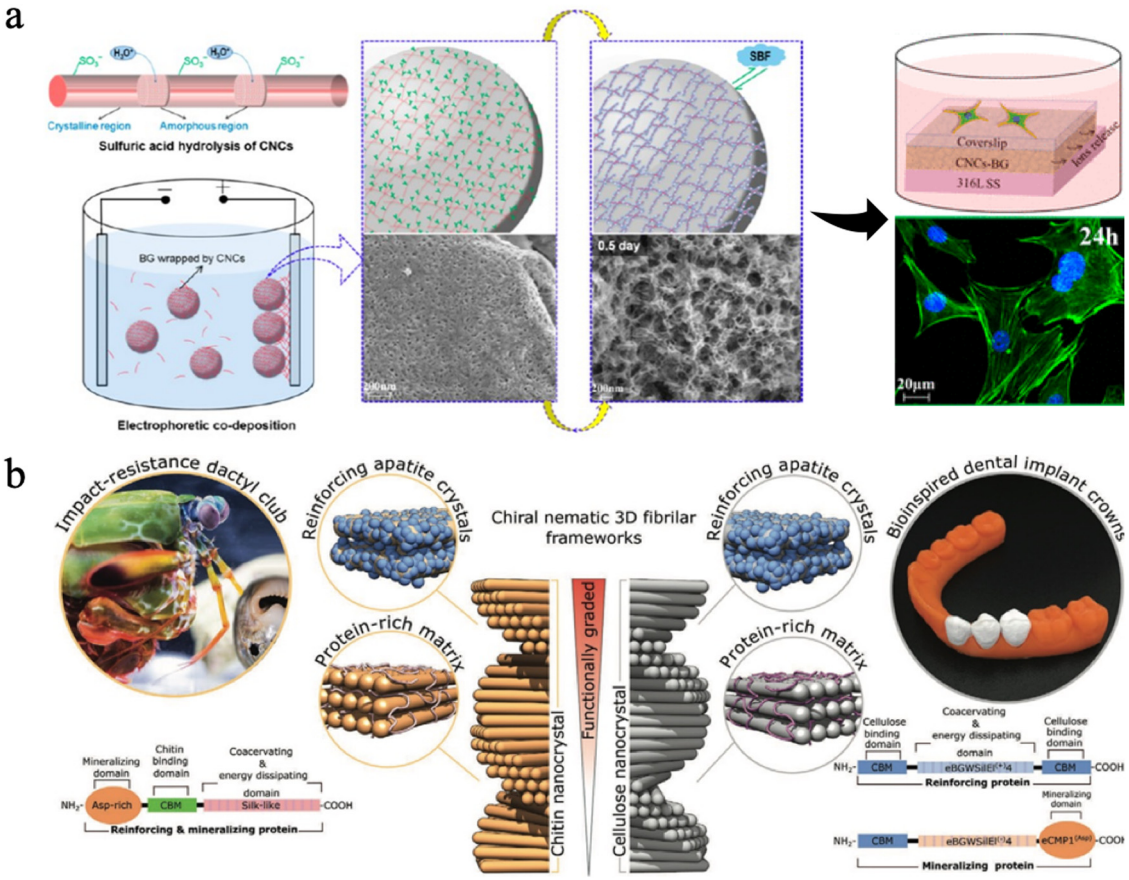

Fig. 12 (a) Design strategy, fabrication of CNC-BG coatings, the SEM images, the confocal fluorescence images and schematic diagrams of cell skeletons on coatings. Reproduced from ref. 230 with permission of the American Chemical Society, copyright 2015. (b) A graded biologically inspired multiphase nanocomposite structure of CNCs mixed with genetically engineered proteins and apatite crystals. Reproduced from ref. 231 with permission from Wiley, copyright 2021.

biomineralized composites such as human teeth,[231] suggesting it has potential in dental applications.

4.2 Soft tissue engineering

Soft tissue engineering has been a research hotspot in tissue regeneration since soft tissue damage or soft tissue-related conditions such as muscle, blood vessels, skin, heart, and cartilage injuries became common in daily clinical work. Natural biopolymers such as polysaccharide-based bio-nanocomposites have extensively attracted scientists due to their great biomimicry and perfect ability to provide biological and physicochemical properties of extracellular matrices. Over recent decades, scientists tried to design new strategies to fabricate multifunctional soft tissue engineering substitutes for repairing damaged soft tissues, providing mechanical support, and killing bacteria simultaneously.[190,191,233] To date, cellulose has been prepared into diverse forms and been modified with different inorganic agents or polymers to develop novel functional biomaterials for soft tissue regeneration.

It is reported that mussels have extraordinary properties such as strong, tough, resistant to bacteria, stable over extreme environments. Xu *et al.* found that iron and the unique hierarchical structure play an essential role in the mussels' mechanical properties.[234] Hence, nanocellulose hybrids with metal or metal oxides or metal–organic-framework structures have also been extensively explored for soft tissue regeneration, especially for wound dressing, which is an intriguing research topic and always discussed in the field of biomaterials. Wang *et al.* designed a copper-containing mesoporous bioactive glass (Cu-MBG) and nanofibrillated cellulose (NFC) composite and co-cultured it with 3T3 fibroblasts, human umbilical vein endothelial cells (HUVECs), and *E. coli.* separately. The biocomposites showed a profound angiogenic effect on 3T3 fibroblasts and HUVECs and an inhibiting effect on the growth of *E. coli.* The biocomposite design based on nanocellulose not only resisted chronic bacterial infection but also promoted angiogenesis.[235] Silver nanoparticles were synthesized into the matrix of CNCs to design wound dressing candidates. The dressings showed water absorption capacity and strong antibacterial activity and gained a synergistic effect on *in vivo* skin wound healing, and documented faster wound closure in treated mice.[236]

TEMPO-oxidized CNF (T-CNF) has low cytotoxicity and structural similarity to extracellular matrices in the form of hydrogels and thus stands out as a platform biomaterial in bioink formulation for 3D printing. Xu *et al.* fabricated a

hydrogel composed of T-CNF and gelatin methacrylate (GelMA) *via in situ* crosslinking by Ca^{2+} and UV. The hydrogel showed non-cytotoxic and biocompatible features of 3T3 fibroblasts and promoted the proliferation of fibroblasts, which exhibits great potential in 3D printing for wound healing applications.[189] In another study, Leppiniemi *et al.* fabricated a stable 3D hydrogel with T-CNF alginate glycerin *via* $CaCl_2$ crosslinking.[237] The T-CNF hydrogel can achieve the printed shape fidelity and stability as the printing paste. The described avidin-functionalized nanocellulose-alginate material provides a generic platform for the immobilization of bioactive components like growth factors or antimicrobial agents such as antibiotics. In addition, the buffer tests demonstrated that the 3D printing of porous structures reduced excess deformation of the objects, especially when the printed structure was cross-linked with $CaCl_2$. Voids within the structure provide room for swelling in moist and wet conditions, thus reducing irritation and pain to accelerate wound healing.[237]

Bacterial cellulose is reported to be more suitable for skin tissue engineering and wound repair. For example, Wu *et al.* demonstrated a BC/lotus root starch/hydroxyapatite (BC/LRS-M/HAp) scaffold endowed with a nanoporous hierarchical structure.[238] The researchers adopted a combinatorial approach to sequentially conduct BC surface modification by LRS, then constructed a 3D architecture by agarose porogen templating with HAp deposition on the BC/LRS-M *via* biomimetic mineralization. The target scaffold had a pore size of 300–500 μm, which was beneficial to cell adhesion and proliferation. Alkaline phosphatase (ALP) activity assay showed a significantly higher ALP activity by approximately 50% and 100% increments, respectively, on BC/LRS-M/HAp than the two control scaffolds. These results suggested that the BC/LRS-M/HAp scaffold could be a great articular cartilage tissue substitute.[238]

4.3 Cancer therapy

It is well known that the intersection between biology and materials science has provided extraordinary natural materials, which cannot be easily synthesized in the laboratory, although it is achieved in nature under ambient conditions without hazardous chemicals. To date, researchers mimicked the process of biomineralization to create abundant biomimetic materials for biological applications. In nature, the biological processes can be divided into biomineralization and remineralization. During remineralization, calcium ions could possibly be deposited anomalously in soft tissues, thus causing pathological diseases.[239,240] However, scientists can promote cancer cell targeting calcification (CTCC) and accelerate cancer cell death to make it a new alternative cancer treatment. Tang *et al.* suggested this novel strategy, and this approach can effectively suppress tumor growth and secondary metastases without destroying normal cells compared to traditional chemotherapy (Fig. 13(a)).[241,242] Epple *et al.* also fabricated calcium phosphate nanoparticles with an inner shell of CMC that incorporates a photoactive dye and an outer shell of poly(ethyleneimine) (PEI).[243] The nanoparticles could be used for photodynamic therapy with HT29 cells (human colon adenocarcinoma cells), HIG-82 cells (rabbit synoviocytes), and J774A.1 cells (murine macrophages) and showed a similar killing efficiency to the pure photoactive dye.[243]

Besides, the mineralization of structures with subcomponents such as metal oxides, silicates, and metal–organic frameworks can be integrated into one single material through chemical modification to cure cancers since nanocellulose has abundant hydroxyl groups. Noorian *et al.* developed a new kind of cellulose fabric combined with the zinc glutamate Bio Metal–Organic Framework (BioMOF) to control the delivery of nitric oxide (NO) and 5-fluorouracil (5FU) for skin cancer therapy.[244] In this material, cellulose acted as a matrix-forming material for long-lasting sustained drug delivery (Fig. 13(b)).[244] Fe_3O_4–Ag_2O quantum dots also were decorated with CNFs for cancer drug delivery. The quantum dots play a role in connecting the cellulose fibers to the anticancer drug etoposide and methotrexate. These multiple hybrid materials have ferromagnetic properties and a constant speed of drug release.[245] Besides, Xu *et al.* utilized carbon quantum dots and cellulose to improve anaerobic digestion.[234]

4.4 Drug, protein, and growth factor delivery

Nanocellulose is promising in medical applications for drug delivery because of its abundant origin, low cost, and biocompatibility. Cellulosic materials have already been made as commercial products for drug delivery. Different drug gradients have been selected to be modified with nanocellulose, thus achieving the goal for therapeutic treatment for different diseases. However, it is still challenging since complicated body environments (*e.g.*, stomach, intestines, bone, cartilage) could limit the drug absorption capacity and curing diseases needs to achieve a long-time, sustainable, and defined amount of drug release.[246] The question of how to achieve exact and efficient drug delivery systems with selective, stable, and controlled release of pharmaceuticals has been a research hotpot. Most specifically, mineralized cellulose-based hydrogel or aerogel scaffolds have been applied for drug delivery due to their high porosity, excellent network structure, and stable mechanical strength. Ryuji *et al.* made a BC/bone cement/antibiotics scaffold to achieve stable antibiotics release and simultaneously high strength. The results showed that the average values for compression strength, fracture toughness, and fatigue life of the cellulose antibiotic cement were 97%, 97%, and 78% of the values obtained for plain cement, respectively. In contrast to these excellent values, the traditional antibiotic cement exhibited only 79% of compression strength, 82% of fracture toughness, and 17% of the fatigue life of plain cement. Moreover, the cumulative elution over 35 days was 129% greater from the cellulose antibiotic cement than from the traditional antibiotic cement. The obtained BC/bone cement/antibiotics improved fatigue life and increased antibiotic elution.[247]

Meanwhile, efforts are dedicated to mixing magnetic or gold nanoparticles as well as two-dimensional materials, into cellulose to obtain efficient drug delivery. Magnetic cellulose (m-CNCs) was synthesized and incorporated into alginate-based hydrogel beads as a potential drug delivery system. The study

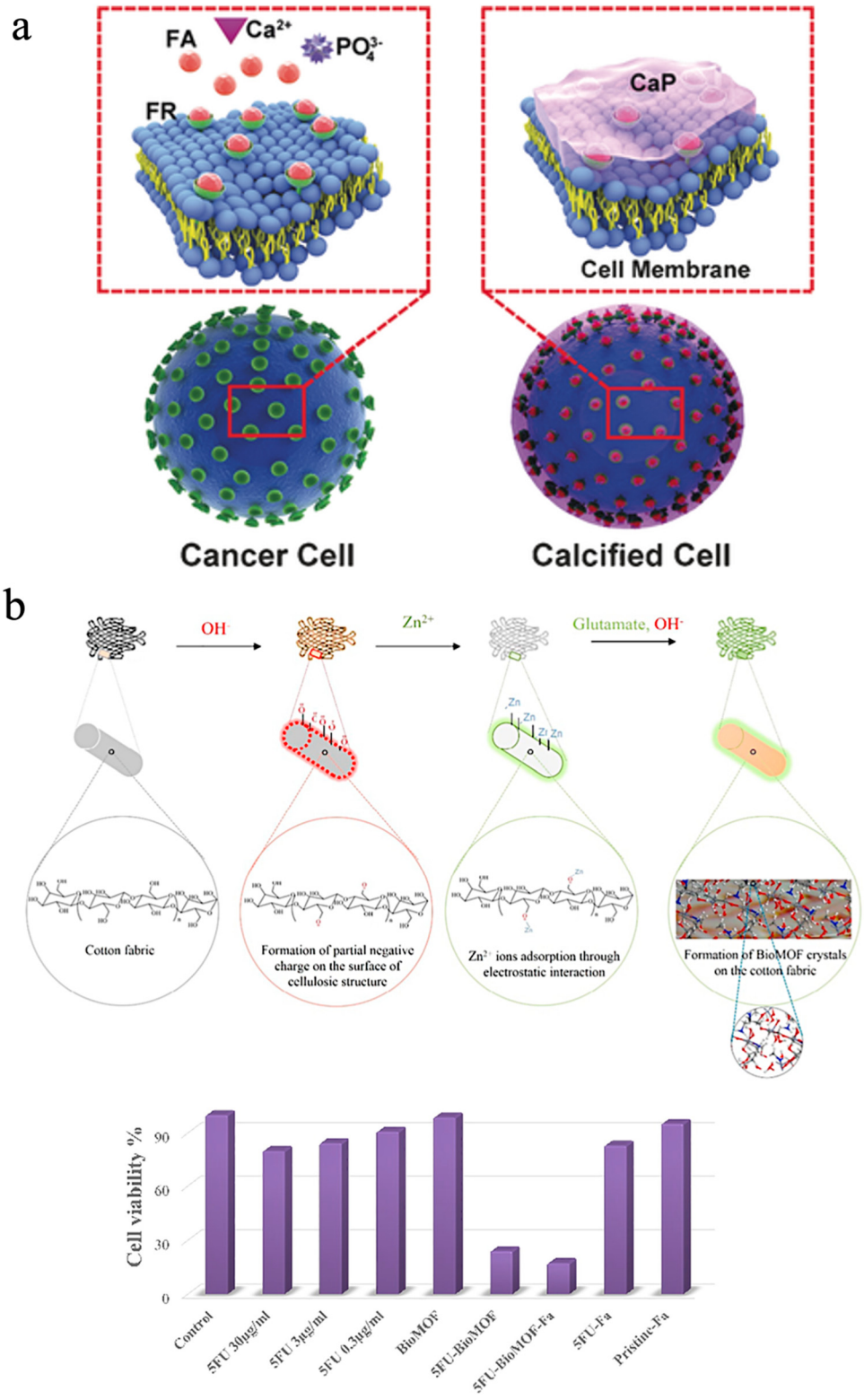

Fig. 13 (a) A scheme of the drug-free tumor therapy strategy *via* biomineralization. Reproduced from ref. 242 with permission of Wiley, copyright 2016. (b) Schematic of *in situ* synthesis of a BioMOF on cotton fabric, and the corresponding cell viability of different groups. Reproduced from ref. 244 with permission of Elsevier, copyright 2019.

showed that m-CNCs could enhance mechanical strength and exhibit controlled release profiles by increasing the integrity of the alginate hydrogel beads and the swelling degree.[248] Sekhar *et al.* developed a novel transdermal device fabricated from a

polyelectrolyte complex (PEC) reinforced with nanogold-nanocellulose (GNP-NC) to enhance the skin permeation of diltiazem hydrochloride.[249] More recently, Luo *et al.*[250] fabricated a novel BC/graphene oxide (GO) nanocomposite drug nanocarrier by embedding GO into a 3D porous network of BC. Ibuprofen (IBU) as a model drug was loaded into the BC/GO nanocomposites. The formed IBU@BC/GO displays a more sustainable release behavior than IBU@BC, which suggests the critical role of GO in promoting the controlled release. Furthermore, *in vitro* cell viability experiments revealed that the BC/GO nanocarrier had many more living cells than BC. It is inferred that the BC/GO nanocarrier could be a great new drug delivery system.

More interestingly, Nishiguchi *et al.*[251] reported an injectable, bioresponsive bone cement composed of bisphosphonate-modified nanocellulose (pNC) and β-tricalcium phosphate (β-TCP). Bisphosphonate is a class of bone resorption inhibitor drug for the treatment of osteoporosis and metastatic bone diseases.[252] The pNC/β-TCP composites mimicked bone structures and possessed various favorable characteristics, including tunable viscoelastic properties, physical binding to the bone, apatite formation, and pH responsiveness. When the pH drops to ~4.5, which corresponded to an osteoclast-induced pH decrease, the pNC-β-TCP composite degraded and released pNC, which suppressed osteoclast formation and pit formation. The injectable bone scaffold of pNC/β-TCP not only enhanced osteoblast differentiation but also regulated osteoclast activity, achieving a dual effect for the treatment of bone diseases and prevention of the locomotive syndrome.

Protein adsorption, protein, and growth factor delivery impact the properties of cellulose and expand the application of cellulose base materials. Fu *et al.* reported a facile and green sonochemical route for the rapid synthesis of cellulose/HA nanocomposites in NaOH/urea aqueous solution. The protein adsorption properties of the as-prepared cellulose/HA nanocomposites are investigated using hemoglobin (Hb) as a model protein. The adsorption of Hb on the surface of cellulose/HA nanocomposites was supported by FT-IR analysis. The peaks located at 1649 cm^{-1} and 1398 cm^{-1} (originating from Hb molecules) occurred after adsorption, indicating that the Hb molecules have been successfully adsorbed on the surface of cellulose/HA nanocomposites. The Hb adsorption properties of the as-prepared cellulose/HA nanocomposites were investigated at different initial Hb concentrations and different amounts of the sample. The amount of adsorbed Hb on the cellulose/HA nanocomposites increases with increasing initial concentration of Hb in the range of 0.2–4.0 mg mL^{-1} and reached 321.5 mg g^{-1} at a Hb initial concentration of 4.0 mg mL^{-1}. The cellulose/HA nanocomposites still did not saturate adsorption at a high Hb concentration of 4.0 mg mL^{-1}, indicating that the cellulose maintained a high protein adsorption capacity after HA mineralization. These results demonstrated that the cellulose/HA nanocomposites could be utilized for application in biomedical fields.[253]

Further research compared the protein adsorption and release ability of mineralized and nonmineralized CMC. Briefly, after calcium phosphate mineralization, the swelling behavior of the CMC-*g*-PDMAEMA hydrogels changes at pH 2.1 and 7.4. The swelling ratio was decreased after calcium phosphate mineralization. This may be due to the fact that inorganic calcium phosphate particles may act as additional crosslinking points between the polymeric chains which hinder the extension of the polymer chains and then suppress the swelling ratio. Moreover, the hybrid takes more time to attain the equilibrium state. Similarly, the BSA loading efficiency is lower in the PDMAEMA/calcium phosphate hybrid. The *in vitro* release of BSA from the CMC-*g*-PDMAEMA hydrogel shows an initial burst release which is possibly due to those BSA that are located near the hydrogel surface. However, the initial burst release of CMC-*g*-PDMAEMA hydrogel is reduced after biomimetic calcium phosphate mineralization. After the burst period, the hydrogel serves as a diffusion barrier and the drug is mainly released by the diffusion mechanism. Compared with the CMC-*g*-PDMEMA hydrogel, the release% was significantly decreased for the CMC-*g*-PDMAEMA/calcium phosphate hybrid at pH 2.1 and 7.4. For example, after 24 h, the release% decreased from 96% to 90% (at pH 2.1) and from 93% to 84% (at pH 7.4) after biomimetic calcium phosphate mineralization. These results suggest the role of mineralized calcium phosphate particles for reducing the permeability of the loaded protein and hence controlling the delivery of protein. These results offer promising multifunctional hybrid materials for bone tissue regeneration.[254]

Ribeiro *et al.* tested the release of the PDGF and VEGF, a chemotactic and a proangiogenic growth factor (GF), respectively, in mineralized and nonmineralized CNC cryogel. Contrary to what would be expected from samples with a higher weight loss, the immunodetection assay showed a decreased release of both GFs in the mineralized groups compared to the control. The more effective entrapment of these GFs in the cryogel scaffolds might result in either the microstructural alterations observed in the material or a favored interaction of these biomolecules with the mineral components. The prolonged bioactivity of the proposed mineralized cellulose cryogel scaffolds provides a new idea for the loading and delivery of proteins and growth factors.[201]

5 Conclusions and outlook

Considering all above-mentioned research, mineralized cellulose has been chosen as a safe, ideal medium to incorporate other active molecules, proteins, polymers, metals or metal oxides to achieve diverse medical applications. In this review, we grasped a comprehensive report of properties, synthesis methods of mineralized nanocellulose and the medical applications, especially in hard tissue engineering. For example, although plenty of studies have focused on hard tissue engineering, we need to incorporate all the important and necessary criteria (such as mechanical properties, natural tissue structure, biocompatibility and physiological properties) into one material. There are still many limitations for mineralized cellulose-related biomaterials to solve.

First, nanocellulose-related tissue engineering substitutes are still a laboratory product. Many efforts need to be spent

on fabricating a uniform, stable, green, biocompatible medical tissue engineering substitute since nanocellulose is reported to dissolve thoroughly in the human body.[255] Second, the strategy of how to best speed up the integration of nanocellulose-related medical products with bone cartilage is still on the way. The underlying mechanism also needs to be explored. Third, mineralized nanocellulose possesses good chemical stability, mechanical tolerance and durability, which may result in complications in bioactive drug molecule delivery. How to balance these properties needs to be resolved to devise personal and intelligent designs for each disease.

Meanwhile, we are still a long way from achieving mineralized cellulose commercialization. There is no doubt that cellulose can be produced from cheap sources and waste materials and this has been commercialized by several companies. However, there are still some shortcomings hindering its clinical application and commercialization. First, the properties of cellulose need to be improved and the application scenarios need to be expanded. Besides, the current technologies for cellulose fabrication at the nanoscale are still expensive, require tedious efforts, and lack large-scale production for industrial and biomedical applications.[256] Thus, it has been shown that modification of properties, increasing yields, a reduction in production costs, and choosing appropriate industrial fabrication lines are the main future goals of researchers.[257] Furthermore, on the path to clinical translational research and clinical translation, the output of nanocellulose with high purity and the absence of endotoxins is highly needed for biomedical applications. Besides, the properties of cellulose should be improved by mixing with other materials, which will bring great possibility for their practical applications in a variety of fields. In addition, there are only limited studies on the toxicity of cellulose in the human body, and a great number of studies are still required to ensure that cellulose is not harmful to human beings.[258] Creating controlled, reliable, and reproducible production techniques will be essential to the ultimate approval of new applications and will help to pave the way for greater acceptance of cellulose as the commercially available material for biomedical translations that it has the possibility to be.[259]

Abbreviations

1D	One-dimensional
HAp	Hydroxyapatite
2D	Two-dimensional
3D	Three-dimensional
NMMO	*N*-Methylmorpholine-*N*-oxide
MC	Methylcellulose
HPC	Hydroxypropyl cellulose
CMC	Carboxymethyl cellulose
DS	Degree of substitution
CNFs	Cellulose nanofibers
CNCs	Cellulose nanocrystals
BC	Bacterial cellulose
TEMPO	2,2,6,6-Tetramethylpiperidine-1-oxyl
LC	Liquid crystal
NPs	Nanoparticles
CF	Cellulose fiber
HAPNWs	HAp nanowires
ZnO	Zinc oxide
MOFs	Metal–organic frameworks
PVP	Polyvinylpyrrolidone
PEG	Polyethylene glycol
PDA	Polydopamine
AuNPs	Gold NPs
QDs	Quantum dots
ALD	Atomic layer deposition
NR	Nanorod
PVA	Poly(vinyl alcohol)
LbL	Layer-by-layer
MTM	Montmorillonite
AC	Aminoclays
PEI	Polyethylenimine
ILs	Ionic liquids
MTMS	Methyltrimethoxysilane
PMSQ	Polymethylsilsesquioxane
CD	Circular dichroism
QNRs	Quantum nanorods
PAA	Polyacrylic acid
SA	Sodium alginate
SBF	Simulated body fluids
CP	Calcium phosphate
Gel	Gelatin
PA	Procyanidin
β-TCP	β-Tricalcium phosphate
PGA	Poly (γ-glutamic acid)
HPMC	(Hydroxypropyl)methyl cellulose
BMSC	Bone mesenchymal stem cell
BG	Bioactive glass
HEC	Hydroxyethyl-cellulose
HUVECs	Human umbilical vein endothelial cells
T-CNF	TEMPO-oxidized CNF
CTCC	Cancer cell targeting calcification
NO	Nitric oxide
5FU	5-Fluorouracil
BioMOF	Bio metal–organic framework
m-CNCs	Magnetic cellulose
GNP-NC	Nanogold-nanocellulose
GO	Graphene oxide
IBU	Ibuprofen
pNC	Bisphosphonate-modified nanocellulose

Conflicts of interest

There are no conflicts to declare.

Acknowledgements

R. X. gratefully acknowledges the funding from the Natural Science Foundation of China (Grant no. 52203142), The Open

Project of State Key Laboratory of New Textile Materials and Advanced Processing Technologies (FZ2021003), and The Joint Project for Talent Innovation Sharing Alliance of Quanzhou (2021C064L). Y. F. gratefully acknowledges the funding from the Shanghai Pujiang Program (22PJD081) and the Fundamental Research Funds for the Centra Universities.

References

1 W. Li, H. Liu, Y. Mi, M. Zhang, J. Shi, M. Zhao, M. A. Ramos, T. S. Hu, J. Li, M. Xu and Q. Xu, *Friction*, 2022, **10**, 80–93.
2 U. G. K. Wegst, H. Bai, E. Saiz, A. P. Tomsia and R. O. Ritchie, *Nat. Mater.*, 2015, **14**, 23–36.
3 E. A. Zimmermann and R. O. Ritchie, *Adv. Healthcare Mater.*, 2015, **4**, 1287–1304.
4 R. O. Ritchie, *Nat. Mater.*, 2011, **10**, 817–822.
5 J. C. Weaver, G. W. Milliron, A. Miserez, K. Evans-Lutterodt, S. Herrera, I. Gallana, W. J. Mershon, B. Swanson, P. Zavattieri, E. DiMasi and D. Kisailus, *Science*, 2012, **336**, 1275–1280.
6 P. Romano, H. Fabritius and D. Raabe, *Acta Biomater.*, 2007, **3**, 301–309.
7 R. Xiong, J. Luan, S. Kang, C. Ye, S. Singamaneni and V. V. Tsukruk, *Chem. Soc. Rev.*, 2020, **49**, 983–1031.
8 B. Yeom, T. Sain, N. Lacevic, D. Bukharina, S.-H. Cha, A. M. Waas, E. M. Arruda and N. A. Kotov, *Nature*, 2017, **543**, 95–98.
9 N. Rauner, M. Meuris, M. Zoric and J. C. Tiller, *Nature*, 2017, **543**, 407–410.
10 H.-L. Gao, S.-M. Chen, L.-B. Mao, Z.-Q. Song, H.-B. Yao, H. Cölfen, X.-S. Luo, F. Zhang, Z. Pan, Y.-F. Meng, Y. Ni and S.-H. Yu, *Nat. Commun.*, 2017, **8**, 287.
11 L.-B. Mao, H.-L. Gao, H.-B. Yao, L. Liu, H. Cölfen, G. Liu, S.-M. Chen, S.-K. Li, Y.-X. Yan, Y.-Y. Liu and S.-H. Yu, *Science*, 2016, **354**, 107–110.
12 M. J. Olszta, X. Cheng, S. S. Jee, R. Kumar, Y.-Y. Kim, M. J. Kaufman, E. P. Douglas and L. B. Gower, *Mater. Sci. Eng., R*, 2007, **58**, 77–116.
13 L. C. Palmer, C. J. Newcomb, S. R. Kaltz, E. D. Spoerke and S. I. Stupp, *Chem. Rev.*, 2008, **108**, 4754–4783.
14 A.-W. Xu, Y. Ma and H. Cölfen, *J. Mater. Chem.*, 2007, **17**, 415–449.
15 F. C. Meldrum and H. Cölfen, *Chem. Rev.*, 2008, **108**, 4332–4432.
16 R. Xiong, A. M. Grant, R. Ma, S. Zhang and V. V. Tsukruk, *Mater. Sci. Eng., R*, 2018, **125**, 1–41.
17 S. Ling, W. Chen, Y. Fan, K. Zheng, K. Jin, H. Yu, M. J. Buehler and D. L. Kaplan, *Prog. Polym. Sci.*, 2018, **85**, 1–56.
18 S. Ling, D. L. Kaplan and M. J. Buehler, *Nat. Rev. Mater.*, 2018, **3**, 1–15.
19 D. Klemm, B. Heublein, H.-P. Fink and A. Bohn, *Angew. Chem., Int. Ed.*, 2005, **44**, 3358–3393.
20 B. Thomas, M. C. Raj, B. AK, H. RM, J. Joy, A. Moores, G. L. Drisko and C. Sanchez, *Chem. Rev.*, 2018, **118**, 11575–11625.
21 D. Klemm, D. Schumann, F. Kramer, N. Heßler, M. Hornung, H.-P. Schmauder and S. Marsch, in *Polysaccharides II*, ed. D. Klemm, Springer, Berlin, Heidelberg, 2006, pp. 49–96.
22 Y. Shchipunov and I. Postnova, *Adv. Funct. Mater.*, 2018, **28**, 1705042.
23 H. Kim, J.-Y. Yi, B.-G. Kim, J. E. Song, H.-J. Jeong and H. R. Kim, *PLoS One*, 2020, **15**, e0233952.
24 C. Pang, R. Shanks and F. Daver, *J. Polym. Eng.*, 2014, **34**, 141–144.
25 E. J. Foster, R. J. Moon, U. P. Agarwal, M. J. Bortner, J. Bras, S. Camarero-Espinosa, K. J. Chan, M. J. D. Clift, E. D. Cranston, S. J. Eichhorn, D. M. Fox, W. Y. Hamad, L. Heux, B. Jean, M. Korey, W. Nieh, K. J. Ong, M. S. Reid, S. Renneckar, R. Roberts, J. A. Shatkin, J. Simonsen, K. Stinson-Bagby, N. Wanasekara and J. Youngblood, *Chem. Soc. Rev.*, 2018, **47**, 2609–2679.
26 P. Makvandi, M. Ghomi, V. V. T. Padil, F. Shalchy, M. Ashrafizadeh, S. Askarinejad, N. Pourreza, A. Zarrabi, E. Nazarzadeh Zare, M. Kooti, B. Mokhtari, A. Borzacchiello and F. R. Tay, *ACS Appl. Nano Mater.*, 2020, **3**, 6210–6238.
27 K. De France, Z. Zeng, T. Wu and G. Nyström, *Adv. Mater.*, 2021, **33**, 2000657.
28 Q. Zhang, L. Zhang, W. Wu and H. Xiao, *Carbohydr. Polym.*, 2020, **229**, 115454.
29 L.-B. Mao, Y.-F. Meng, X.-S. Meng, B. Yang, Y.-L. Yang, Y.-J. Lu, Z.-Y. Yang, L.-M. Shang and S.-H. Yu, *J. Am. Chem. Soc.*, 2022, **144**, 18175–18194.
30 L. Valencia, R. Handa, S. Monti, A. B. Jasso-Salcedo, D. Georgouvelas, I. Magaña, R. D. de León, K. P. Velikov, A. P. Mathew and S. Kumar, *J. Mater. Chem. A*, 2022, **10**, 9248–9276.
31 R. J. Moon, A. Martini, J. Nairn, J. Simonsen and J. Youngblood, *Chem. Soc. Rev.*, 2011, **40**, 3941–3994.
32 H. P. S. Abdul Khalil, A. H. Bhat and A. F. Ireana Yusra, *Carbohydr. Polym.*, 2012, **87**, 963–979.
33 S. Vignolini, P. J. Rudall, A. V. Rowland, A. Reed, E. Moyroud, R. B. Faden, J. J. Baumberg, B. J. Glover and U. Steiner, *Proc. Natl. Acad. Sci. U. S. A.*, 2012, **109**, 15712–15715.
34 H. Zhu, W. Luo, P. N. Ciesielski, Z. Fang, J. Y. Zhu, G. Henriksson, M. E. Himmel and L. Hu, *Chem. Rev.*, 2016, **116**, 9305–9374.
35 C. Chen, Y. Kuang, S. Zhu, I. Burgert, T. Keplinger, A. Gong, T. Li, L. Berglund, S. J. Eichhorn and L. Hu, *Nat. Rev. Mater.*, 2020, **5**, 642–666.
36 D. Miyashiro, R. Hamano and K. Umemura, *Nanomaterials*, 2020, **10**, 186.
37 L. K. J. Hauru, M. Hummel, K. Nieminen, A. Michud and H. Sixta, *Soft Matter*, 2016, **12**, 1487–1495.
38 Q. Yang, H. Fukuzumi, T. Saito, A. Isogai and L. Zhang, *Biomacromolecules*, 2011, **12**, 2766–2771.
39 J. Zhou, C. Chang, R. Zhang and L. Zhang, *Macromol. Biosci.*, 2007, **7**, 804–809.
40 S. Wang, A. Lu and L. Zhang, *Prog. Polym. Sci.*, 2016, **53**, 169–206.

41 H. Wang, G. Gurau and R. D. Rogers, *Chem. Soc. Rev.*, 2012, **41**, 1519–1537.
42 A. Pinkert, K. N. Marsh, S. Pang and M. P. Staiger, *Chem. Rev.*, 2009, **109**, 6712–6728.
43 H. Tu, X. Li, Y. Liu, L. Luo, B. Duan and R. Zhang, *Carbohydr. Polym.*, 2022, **296**, 119942.
44 W. Ge, J. Shuai, Y. Wang, Y. Zhou and X. Wang, *Polym. Chem.*, 2022, **13**, 359–372.
45 D. Wallick, in *Microencapsulation in the Food Industry*, ed. A. G. Gaonkar, N. Vasisht, A. R. Khare and R. Sobel, Academic Press, San Diego, 2014, pp. 181–193.
46 M. H. Godinho, D. G. Gray and P. Pieranski, *Liq. Cryst.*, 2017, **44**, 2108–2120.
47 D. Klemm, F. Kramer, S. Moritz, T. Lindström, M. Ankerfors, D. Gray and A. Dorris, *Angew. Chem., Int. Ed.*, 2011, **50**, 5438–5466.
48 T. Rosén, H. He, R. Wang, C. Zhan, S. Chodankar, A. Fall, C. Aulin, P. T. Larsson, T. Lindström and B. S. Hsiao, *ACS Nano*, 2020, **14**, 16743–16754.
49 H. P. S. Abdul Khalil, Y. Davoudpour, Md. N. Islam, A. Mustapha, K. Sudesh, R. Dungani and M. Jawaid, *Carbohydr. Polym.*, 2014, **99**, 649–665.
50 W. Chen, Q. Li, Y. Wang, X. Yi, J. Zeng, H. Yu, Y. Liu and J. Li, *ChemSusChem*, 2014, **7**, 154–161.
51 T. Saito, S. Kimura, Y. Nishiyama and A. Isogai, *Biomacromolecules*, 2007, **8**, 2485–2491.
52 A. Isogai, T. Saito and H. Fukuzumi, *Nanoscale*, 2011, **3**, 71–85.
53 A. Isogai, *Adv. Mater.*, 2021, **33**, 2000630.
54 Y. Habibi, L. A. Lucia and O. J. Rojas, *Chem. Rev.*, 2010, **110**, 3479–3500.
55 T. G. Parton, R. M. Parker, G. T. van de Kerkhof, A. Narkevicius, J. S. Haataja, B. Frka-Petesic and S. Vignolini, *Nat. Commun.*, 2022, **13**, 2657.
56 R. M. Parker, G. Guidetti, C. A. Williams, T. Zhao, A. Narkevicius, S. Vignolini and B. Frka-Petesic, *Adv. Mater.*, 2018, **30**, 1704477.
57 C. Wang, C. Tang, Y. Wang, Y. Shen, W. Qi, T. Zhang, R. Su and Z. He, *Curr. Opin. Solid State Mater. Sci.*, 2022, **26**, 101017.
58 A. Tran, C. E. Boott and M. J. MacLachlan, *Adv. Mater.*, 2020, **32**, 1905876.
59 J. Wang, J. Tavakoli and Y. Tang, *Carbohydr. Polym.*, 2019, **219**, 63–76.
60 Y. Huang, C. Zhu, J. Yang, Y. Nie, C. Chen and D. Sun, *Cellulose*, 2014, **21**, 1–30.
61 M. A. Hubbe, R. A. Venditti and O. J. Rojas, *BioResources*, 2007, **2**, 739–788.
62 S. Ge, L. Zhang, Y. Zhang, F. Lan, M. Yan and J. Yu, *Nanoscale*, 2017, **9**, 4366–4382.
63 Z. Weng, Y. Su, D.-W. Wang, F. Li, J. Du and H.-M. Cheng, *Adv. Energy Mater.*, 2011, **1**, 917–922.
64 A. T. Vicente, A. Araújo, M. J. Mendes, D. Nunes, M. J. Oliveira, O. Sanchez-Sobrado, M. P. Ferreira, H. Águas, E. Fortunato and R. Martins, *J. Mater. Chem. C*, 2018, **6**, 3143–3181.
65 F.-F. Chen, Z.-H. Dai, Y.-N. Feng, Z.-C. Xiong, Y.-J. Zhu and Y. Yu, *ACS Nano*, 2021, **15**, 5355–5365.
66 T. J. Athauda, U. Butt and R. R. Ozer, *RSC Adv.*, 2013, **3**, 21431–21438.
67 X. Yue, T. Zhang, D. Yang, F. Qiu and Z. Li, *Cellulose*, 2018, **25**, 5951–5965.
68 L. Zhu, L. Zong, X. Wu, M. Li, H. Wang, J. You and C. Li, *ACS Nano*, 2018, **12**, 4462–4468.
69 S.-C. Li, B.-C. Hu, L.-M. Shang, T. Ma, C. Li, H.-W. Liang and S.-H. Yu, *Adv. Mater.*, 2022, **34**, 2202504.
70 X. Wu, C. Lu, Z. Zhou, G. Yuan, R. Xiong and X. Zhang, *Environ. Sci.: Nano*, 2014, **1**, 71–79.
71 X. Wu, C. Lu, W. Zhang, G. Yuan, R. Xiong and X. Zhang, *J. Mater. Chem. A*, 2013, **1**, 8645–8652.
72 R. Xiong, C. Lu, Y. Wang, Z. Zhou and X. Zhang, *J. Mater. Chem. A*, 2013, **1**, 14910–14918.
73 R. Xiong, C. Lu, W. Zhang, Z. Zhou and X. Zhang, *Carbohydr. Polym.*, 2013, **95**, 214–219.
74 S. Ifuku, M. Tsuji, M. Morimoto, H. Saimoto and H. Yano, *Biomacromolecules*, 2009, **10**, 2714–2717.
75 Z. Ma, J. Liu, G. Shen, X. Zheng, Y. Pei and K. Tang, *Cellulose*, 2021, **28**, 6287–6303.
76 S. Galland, R. L. Andersson, M. Salajková, V. Ström, R. T. Olsson and L. A. Berglund, *J. Mater. Chem. C*, 2013, **1**, 7963–7972.
77 C. Katepetch and R. Rujiravanit, *Carbohydr. Polym.*, 2011, **86**, 162–170.
78 M. Sureshkumar, D. Yovita Siswanto and C.-K. Lee, *J. Mater. Chem.*, 2010, **20**, 6948–6955.
79 Y. Li, H. Zhu, H. Gu, H. Dai, Z. Fang, N. J. Weadock, Z. Guo and L. Hu, *J. Mater. Chem. A*, 2013, **1**, 15278–15283.
80 Y.-M. Ju, Y. Zhao, Q.-F. Guan, S.-Y. Yang, W. Wang, B.-B. Yan, Y.-F. Meng, S.-C. Li, P.-P. Tang, L.-B. Mao and S.-H. Yu, *Angew. Chem., Int. Ed.*, 2022, e202211254.
81 J. Majoinen, J. Hassinen, J. S. Haataja, H. T. Rekola, E. Kontturi, M. A. Kostiainen, R. H. A. Ras, P. Törmä and O. Ikkala, *Adv. Mater.*, 2016, **28**, 5262–5267.
82 T. Abitbol, H. S. Marway, S. A. Kedzior, X. Yang, A. Franey, D. G. Gray and E. D. Cranston, *Cellulose*, 2017, **24**, 1287–1293.
83 S. Morimune-Moriya, M. Salajkova, Q. Zhou, T. Nishino and L. A. Berglund, *Biomacromolecules*, 2018, **19**, 2423–2431.
84 A. N. Fernandes, L. H. Thomas, C. M. Altaner, P. Callow, V. T. Forsyth, D. C. Apperley, C. J. Kennedy and M. C. Jarvis, *Proc. Natl. Acad. Sci. U. S. A.*, 2011, **108**, E1195–E1203.
85 Y. Li, H. Zhu, F. Shen, J. Wan, S. Lacey, Z. Fang, H. Dai and L. Hu, *Nano Energy*, 2015, **13**, 346–354.
86 R. Sinko, X. Qin and S. Keten, *MRS Bull.*, 2015, **40**, 340–348.
87 R. Xiong, H. S. Kim, L. Zhang, V. F. Korolovych, S. Zhang, Y. G. Yingling and V. V. Tsukruk, *Angew. Chem., Int. Ed.*, 2018, **57**, 8508–8513.
88 A. Hajian, S. B. Lindström, T. Pettersson, M. M. Hamedi and L. Wågberg, *Nano Lett.*, 2017, **17**, 1439–1447.
89 Q. Li, Z. Xue, J. Zhao, C. Ao, X. Jia, T. Xia, Q. Wang, X. Deng, W. Zhang and C. Lu, *Chem. Eng. J.*, 2020, **383**, 123101.

90 C. Marichy, M. Bechelany and N. Pinna, *Adv. Mater.*, 2012, **24**, 1017–1032.
91 M. E. Lamm, K. Li, J. Qian, L. Wang, N. Lavoine, R. Newman, D. J. Gardner, T. Li, L. Hu, A. J. Ragauskas, H. Tekinalp, V. Kunc and S. Ozcan, *Adv. Mater.*, 2021, **33**, 2005538.
92 J. T. Korhonen, P. Hiekkataipale, J. Malm, M. Karppinen, O. Ikkala and R. H. A. Ras, *ACS Nano*, 2011, **5**, 1967–1974.
93 Z. Li, C. Yao, F. Wang, Z. Cai and X. Wang, *Nanotechnology*, 2014, **25**, 504005.
94 W. J. Landis, K. J. Hodgens, J. Arena, M. J. Song and B. F. McEwen, *Microsc. Res. Tech.*, 1996, **33**, 192–202.
95 S. Iwamoto, A. Isogai and T. Iwata, *Biomacromolecules*, 2011, **12**, 831–836.
96 N. Mittal, F. Ansari, K. G. V, C. Brouzet, P. Chen, P. T. Larsson, S. V. Roth, F. Lundell, L. Wågberg, N. A. Kotov and L. D. Söderberg, *ACS Nano*, 2018, **12**, 6378–6388.
97 A. Walther, J. V. I. Timonen, I. Díez, A. Laukkanen and O. Ikkala, *Adv. Mater.*, 2011, **23**, 2924–2928.
98 Y. Qi, Z. Cheng, Z. Ye, H. Zhu and C. Aparicio, *ACS Appl. Mater. Interfaces*, 2019, **11**, 27598–27604.
99 Z. Cheng, Z. Ye, A. Natan, Y. Ma, H. Li, Y. Chen, L. Wan, C. Aparicio and H. Zhu, *ACS Appl. Mater. Interfaces*, 2019, **11**, 42486–42495.
100 H. Zhao, S. Liu, Y. Wei, Y. Yue, M. Gao, Y. Li, X. Zeng, X. Deng, N. A. Kotov, L. Guo and L. Jiang, *Science*, 2022, **375**, 551–556.
101 F. Guan, Y. Xie, H. Wu, Y. Meng, Y. Shi, M. Gao, Z. Zhang, S. Chen, Y. Chen, H. Wang and Q. Pei, *ACS Nano*, 2020, **14**, 15428–15439.
102 F. Barthelat, Z. Yin and M. J. Buehler, *Nat. Rev. Mater.*, 2016, **1**, 1–16.
103 Z. Sun, T. Liao, W. Li, Y. Qiao and K. (Ken) Ostrikov, *Adv. Funct. Mater.*, 2019, **29**, 1901460.
104 J. Gim, N. Schnitzer, L. M. Otter, Y. Cui, S. Motreuil, F. Marin, S. E. Wolf, D. E. Jacob, A. Misra and R. Hovden, *Nat. Commun.*, 2019, **10**, 4822.
105 A. P. Jackson, J. F. V. Vincent, R. M. Turner and R. M. Alexander, *Proc. R. Soc. London, Ser. B*, 1988, **234**, 415–440.
106 F. Barthelat, H. Tang, P. D. Zavattieri, C.-M. Li and H. D. Espinosa, *J. Mech. Phys. Solids*, 2007, **55**, 306–337.
107 B. Wijerathne, T. Liao, K. (Ken) Ostrikov and Z. Sun, *Small Struct.*, 2022, **3**, 2100228.
108 P. Das, H. Thomas, M. Moeller and A. Walther, *Sci. Rep.*, 2017, **7**, 39910.
109 Y. Liu, S.-H. Yu and L. Bergström, *Adv. Funct. Mater.*, 2018, **28**, 1703277.
110 H.-B. Yao, J. Ge, L.-B. Mao, Y.-X. Yan and S.-H. Yu, *Adv. Mater.*, 2014, **26**, 163–188.
111 K. Wu, J. Fang, J. Ma, R. Huang, S. Chai, F. Chen and Q. Fu, *ACS Appl. Mater. Interfaces*, 2017, **9**, 30035–30045.
112 H. Tu, K. Xie, X. Lin, R. Zhang, F. Chen, Q. Fu, B. Duan and L. Zhang, *J. Mater. Chem. A*, 2021, **9**, 10304–10315.
113 W. Tian, A. VahidMohammadi, M. S. Reid, Z. Wang, L. Ouyang, J. Erlandsson, T. Pettersson, L. Wågberg, M. Beidaghi and M. M. Hamedi, *Adv. Mater.*, 2019, **31**, 1902977.
114 S. Cao, L. Shi, M. Miao, J. Fang, H. Zhao and X. Feng, *Electrochim. Acta*, 2019, **298**, 22–30.
115 Y. Levi-Kalisman, G. Falini, L. Addadi and S. Weiner, *J. Struct. Biol.*, 2001, **135**, 8–17.
116 J. Wang, Q. Cheng, L. Lin and L. Jiang, *ACS Nano*, 2014, **8**, 2739–2745.
117 P. Laaksonen, A. Walther, J.-M. Malho, M. Kainlauri, O. Ikkala and M. B. Linder, *Angew. Chem., Int. Ed.*, 2011, **50**, 8688–8691.
118 A. Walther, I. Bjurhager, J.-M. Malho, J. Ruokolainen, L. Berglund and O. Ikkala, *Angew. Chem., Int. Ed.*, 2010, **49**, 6448–6453.
119 A. Walther, I. Bjurhager, J.-M. Malho, J. Pere, J. Ruokolainen, L. A. Berglund and O. Ikkala, *Nano Lett.*, 2010, **10**, 2742–2748.
120 H.-B. Yao, Z.-H. Tan, H.-Y. Fang and S.-H. Yu, *Angew. Chem., Int. Ed.*, 2010, **49**, 10127–10131.
121 J. J. Richardson, M. Björnmalm and F. Caruso, *Science*, 2015, **348**, aaa2491.
122 M. Farhadi-Khouzani, C. Schütz, G. M. Durak, J. Fornell, J. Sort, G. Salazar-Alvarez, L. Bergström and D. Gebauer, *J. Mater. Chem. A*, 2017, **5**, 16128–16133.
123 P. Tzeng, D. J. Hewson, P. Vukusic, S. J. Eichhorn and J. C. Grunlan, *J. Mater. Chem. C*, 2015, **3**, 4260–4264.
124 Z. Jia, Z. Deng and L. Li, *Adv. Mater.*, 2022, **34**, 2106259.
125 W. Huang, M. Shishehbor, N. Guarín-Zapata, N. D. Kirchhofer, J. Li, L. Cruz, T. Wang, S. Bhowmick, D. Stauffer, P. Manimunda, K. N. Bozhilov, R. Caldwell, P. Zavattieri and D. Kisailus, *Nat. Mater.*, 2020, **19**, 1236–1243.
126 K. Markstedt, J. Sundberg and P. Gatenholm, *3D Print. Addit. Manuf.*, 2014, **1**, 115–121.
127 J. S. Park, T. Kim and W. S. Kim, *Sci. Rep.*, 2017, **7**, 3246.
128 K. Markstedt, A. Mantas, I. Tournier, H. Martínez Ávila, D. Hägg and P. Gatenholm, *Biomacromolecules*, 2015, **16**, 1489–1496.
129 A. Sydney Gladman, E. A. Matsumoto, R. G. Nuzzo, L. Mahadevan and J. A. Lewis, *Nat. Mater.*, 2016, **15**, 413–418.
130 L. Dai, T. Cheng, C. Duan, W. Zhao, W. Zhang, X. Zou, J. Aspler and Y. Ni, *Carbohydr. Polym.*, 2019, **203**, 71–86.
131 G. Siqueira, D. Kokkinis, R. Libanori, M. K. Hausmann, A. S. Gladman, A. Neels, P. Tingaut, T. Zimmermann, J. A. Lewis and A. R. Studart, *Adv. Funct. Mater.*, 2017, **27**, 1604619.
132 M. K. Hausmann, P. A. Rühs, G. Siqueira, J. Läuger, R. Libanori, T. Zimmermann and A. R. Studart, *ACS Nano*, 2018, **12**, 6926–6937.
133 V. Saxena, A. Hasan and L. M. Pandey, *Cellulose*, 2021, **28**, 9207–9226.
134 D. Kharaghani, D. Dutta, K. K. K. Ho, K.-Q. Zhang, W. Kai, X. Ren, M. D. P. Willcox and I. S. Kim, *Cellulose*, 2020, **27**, 3319–3334.
135 A. M. Cakmak, S. Unal, A. Sahin, F. N. Oktar, M. Sengor, N. Ekren, O. Gunduz and D. M. Kalaskar, *Polymers*, 2020, **12**, 1962.

136 S. Guerzoni, H. Deplaine, J. El Haskouri, P. Amorós, M. M. Pradas, U. Edlund and G. G. Ferrer, *J. Bioact. Compat. Polym.*, 2014, **29**, 15–31.
137 A. Salama, *Int. J. Biol. Macromol.*, 2019, **127**, 606–617.
138 A. Xin, Y. Su, S. Feng, M. Yan, K. Yu, Z. Feng, K. Hoon Lee, L. Sun and Q. Wang, *Adv. Mater.*, 2021, **33**, 2006946.
139 G. Chen, X. Liang, P. Zhang, S. Lin, C. Cai, Z. Yu and J. Liu, *Adv. Funct. Mater.*, 2022, **32**, 2113262.
140 R. E. Abouzeid, R. Khiari, D. Beneventi and A. Dufresne, *Biomacromolecules*, 2018, **19**, 4442–4452.
141 J. G. Torres-Rendon, T. Femmer, L. De Laporte, T. Tigges, K. Rahimi, F. Gremse, S. Zafarnia, W. Lederle, S. Ifuku, M. Wessling, J. G. Hardy and A. Walther, *Adv. Mater.*, 2015, **27**, 2989–2995.
142 U. G. K. Wegst, M. Schecter, A. E. Donius and P. M. Hunger, *Philos. Trans. R. Soc., A*, 2010, **368**, 2099–2121.
143 Q. Cheng, C. Huang and A. P. Tomsia, *Adv. Mater.*, 2017, **29**, 1703155.
144 S. Deville, *Adv. Eng. Mater.*, 2008, **10**, 155–169.
145 B. Wicklein, A. Kocjan, G. Salazar-Alvarez, F. Carosio, G. Camino, M. Antonietti and L. Bergström, *Nat. Nanotechnol.*, 2015, **10**, 277–283.
146 Z. Zeng, T. Wu, D. Han, Q. Ren, G. Siqueira and G. Nyström, *ACS Nano*, 2020, **14**, 2927–2938.
147 Y. Chen, D. Fan, S. Lyu, G. Li, F. Jiang and S. Wang, *ACS Sustainable Chem. Eng.*, 2019, **7**, 1381–1388.
148 P. Munier, V. Apostolopoulou-Kalkavoura, M. Persson and L. Bergström, *Cellulose*, 2020, **27**, 10825–10836.
149 F. Carosio, L. Medina, J. Kochumalayil and L. A. Berglund, *Adv. Mater. Interfaces*, 2021, **8**, 2101111.
150 K. J. De France, T. Hoare and E. D. Cranston, *Chem. Mater.*, 2017, **29**, 4609–4631.
151 M. Chau, K. J. De France, B. Kopera, V. R. Machado, S. Rosenfeldt, L. Reyes, K. J. W. Chan, S. Förster, E. D. Cranston, T. Hoare and E. Kumacheva, *Chem. Mater.*, 2016, **28**, 3406–3415.
152 P. Munier, K. Gordeyeva, L. Bergström and A. B. Fall, *Biomacromolecules*, 2016, **17**, 1875–1881.
153 Z. Zeng, C. Wang, G. Siqueira, D. Han, A. Huch, S. Abdolhosseinzadeh, J. Heier, F. Nüesch, C. (John) Zhang and G. Nyström, *Adv. Sci.*, 2020, **7**, 2000979.
154 Z. Zeng, E. Mavrona, D. Sacré, N. Kummer, J. Cao, L. A. E. Müller, E. Hack, P. Zolliker and G. Nyström, *ACS Nano*, 2021, **15**, 7451–7462.
155 S. Ahankari, P. Paliwal, A. Subhedar and H. Kargarzadeh, *ACS Nano*, 2021, **15**, 3849–3874.
156 C. Liu, L. Wan, Q. Li, X. Sun, A. Natan, D. Cao, P. Luan and H. Zhu, *ACS Appl. Polym. Mater.*, 2021, **3**, 1358–1367.
157 L. Wan, C. Liu, D. Cao, X. Sun and H. Zhu, *ACS Appl. Polym. Mater.*, 2020, **2**, 3001–3009.
158 J. Zhang, Y. Cheng, C. Xu, M. Gao, M. Zhu and L. Jiang, *Adv. Funct. Mater.*, 2021, **31**, 2009349.
159 U. G. Wegst, H. Bai, E. Saiz, A. P. Tomsia and R. O. Ritchie, *Nat. Mater.*, 2015, **14**, 23.
160 Y. Yang, Z. Chen, X. Song, Z. Zhang, J. Zhang, K. K. Shung, Q. Zhou and Y. Chen, *Adv. Mater.*, 2017, **29**, 1605750.
161 S.-M. Chen, H.-L. Gao, Y.-B. Zhu, H.-B. Yao, L.-B. Mao, Q.-Y. Song, J. Xia, Z. Pan, Z. He, H.-A. Wu and S.-H. Yu, *Natl. Sci. Rev.*, 2018, **5**, 703–714.
162 R. M. Erb, R. Libanori, N. Rothfuchs and A. R. Studart, *Science*, 2012, **335**, 199–204.
163 R. Xiong, A. M. Grant, R. Ma, S. Zhang and V. V. Tsukruk, *Mater. Sci. Eng., R*, 2018, **125**, 1–41.
164 J. P. F. Lagerwall, C. Schütz, M. Salajkova, J. Noh, J. Hyun Park, G. Scalia and L. Bergström, *NPG Asia Mater.*, 2014, **6**, e80.
165 S. Kang, G. M. Biesold, H. Lee, D. Bukharina, Z. Lin and V. V. Tsukruk, *Adv. Funct. Mater.*, 2021, **31**, 2104596.
166 M. Xu, C. Ma, J. Zhou, Y. Liu, X. Wu, S. Luo, W. Li, H. Yu, Y. Wang, Z. Chen, J. Li and S. Liu, *J. Mater. Chem. C*, 2019, **7**, 13794–13802.
167 T.-D. Nguyen, W. Y. Hamad and M. J. MacLachlan, *Adv. Funct. Mater.*, 2014, **24**, 777–783.
168 T. Zhang, C. Tang, Y. Wang, C. Wang, Y. Zhang, W. Qi, R. Su and Z. He, *Langmuir*, 2022, **38**, 4147–4155.
169 D. Qu, J. Zhang, G. Chu, H. Jiang, C. Wu and Y. Xu, *J. Mater. Chem. C*, 2016, **4**, 1764–1768.
170 A. Querejeta-Fernández, G. Chauve, M. Methot, J. Bouchard and E. Kumacheva, *J. Am. Chem. Soc.*, 2014, **136**, 4788–4793.
171 Z. Cheng, Y. Ma, L. Yang, F. Cheng, Z. Huang, A. Natan, H. Li, Y. Chen, D. Cao, Z. Huang, Y. Wang, Y. Liu, R. Yang and H. Zhu, *Adv. Opt. Mater.*, 2019, **7**, 1801816.
172 R. Xiong, W. Wu, C. Lu and H. Cölfen, *Adv. Mater.*, 2022, **34**, 2206509.
173 L. A. Berglund and I. Burgert, *Adv. Mater.*, 2018, **30**, 1704285.
174 H. Zhou, D. Wen, X. Hao, C. Chen, N. Zhao, R. Ou and Q. Wang, *Chem. Eng. J.*, 2023, **451**, 138308.
175 C. Mai and H. Militz, *Wood Sci. Technol.*, 2004, **37**, 453–461.
176 S. Donath, H. Militz and C. Mai, *Wood Sci. Technol.*, 2004, **38**, 555–566.
177 V. Merk, M. Chanana, N. Gierlinger, A. M. Hirt and I. Burgert, *ACS Appl. Mater. Interfaces*, 2014, **6**, 9760–9767.
178 V. Merk, M. Chanana, T. Keplinger, S. Gaan and I. Burgert, *Green Chem.*, 2015, **17**, 1423–1428.
179 A. Kumar, T. Jyske and M. Petrič, *Adv. Sustainable Syst.*, 2021, **5**, 2000251.
180 W. Kong, C. Wang, C. Jia, Y. Kuang, G. Pastel, C. Chen, G. Chen, S. He, H. Huang, J. Zhang, S. Wang and L. Hu, *Adv. Mater.*, 2018, **30**, 1801934.
181 Y. Li, E. Vasileva, I. Sychugov, S. Popov and L. Berglund, *Adv. Opt. Mater.*, 2018, **6**, 1800059.
182 X. Zhang, B. Wu, S. Sun and P. Wu, *Adv. Funct. Mater.*, 2020, **30**, 1910425.
183 X. Wang, J. Fang, W. Zhu, C. Zhong, D. Ye, M. Zhu, X. Lu, Y. Zhao and F. Ren, *Adv. Funct. Mater.*, 2021, **31**, 2010068.
184 C. A. López, G. Bellesia, A. Redondo, P. Langan, S. P. S. Chundawat, B. E. Dale, S. J. Marrink and S. Gnanakaran, *J. Phys. Chem. B*, 2015, **119**, 465–473.
185 N. Mittal, F. Ansari, K. G. V, C. Brouzet, P. Chen, P. T. Larsson, S. V. Roth, F. Lundell, L. Wågberg, N. A. Kotov and L. D. Söderberg, *ACS Nano*, 2018, **12**, 6378–6388.

186 D. Nepal, S. Kang, K. M. Adstedt, K. Kanhaiya, M. R. Bockstaller, L. C. Brinson, M. J. Buehler, P. V. Coveney, K. Dayal, J. A. El-Awady, L. C. Henderson, D. L. Kaplan, S. Keten, N. A. Kotov, G. C. Schatz, S. Vignolini, F. Vollrath, Y. Wang, B. I. Yakobson, V. V. Tsukruk and H. Heinz, *Nat. Mater.*, 2023, **22**, 18–35.
187 J. Wang, Q. Liu, Z. Guo, H. Pan, Z. Liu and R. Tang, *ACS Biomater. Sci. Eng.*, 2022, **8**, 484–492.
188 K. Li, C. M. Clarkson, L. Wang, Y. Liu, M. Lamm, Z. Pang, Y. Zhou, J. Qian, M. Tajvidi, D. J. Gardner, H. Tekinalp, L. Hu, T. Li, A. J. Ragauskas, J. P. Youngblood and S. Ozcan, *ACS Nano*, 2021, **15**, 3646–3673.
189 W. Xu, B. Z. Molino and F. Cheng, *ACS Appl. Mater. Interfaces*, 2019, **11**, 8838–8848.
190 J. Li, R. Cha and K. Mou, *Adv. Healthcare Mater.*, 2018, **7**, 1800334.
191 H. Shokrani, A. Shokrani and M. Jouyandeh, *ACS Appl. Bio Mater.*, 2022, **5**, 2107–2121.
192 C. Chen, W. Ding, H. Zhang, L. Zhang, Y. Huang, M. Fan, J. Yang and D. Sun, *Carbohydr. Polym.*, 2022, **278**, 118995.
193 M. Pang, Y. Huang, F. Meng, Y. Zhuang, H. Liu, M. Du, Q. Ma, Q. Wang, Z. Chen, L. Chen, T. Cai and Y. Cai, *Eur. Polym. J.*, 2020, **122**, 109365.
194 J. Ravoor, M. Thangavel and E. S. R, *ACS Appl. Bio Mater.*, 2021, **4**, 8129–8158.
195 W. Liu, H. Du and M. Zhang, *ACS Sustainable Chem. Eng.*, 2020, **8**, 7536–7562.
196 B. L. Tardy, B. D. Mattos, C. G. Otoni, M. Beaumont, J. Majoinen, T. Kamarainen and O. J. Rojas, *Chem. Rev.*, 2021, **121**, 14088–14188.
197 Q. F. Guan, Z. M. Han, Z. C. Ling, H. B. Yang and S. H. Yu, *Acc. Mater. Res.*, 2022, **3**, 608–619.
198 P. Makvandi, M. Ghomi and V. V. T. Padil, *ACS Appl. Nano Mater.*, 2020, **3**, 6210–6238.
199 M. Ojansivu, A. Rashad and A. Ahlinder, *Biofabrication*, 2019, **11**, 035010.
200 G. Wang, T. Lu, X. Zhang, M. Feng, C. Wang, W. Yao, S. Zhou, Z. Zhu, W. Ding and M. He, *Int. J. Biol. Macromol.*, 2021, **186**, 377–384.
201 J. P. Ribeiro, R. M. A. Domingues, P. S. Babo, L. P. Nogueira, J. E. Reseland, R. L. Reis, M. Gomez-Florit and M. E. Gomes, *Carbohydr. Polym.*, 2022, **292**, 119638.
202 K. A. Zimmermann, J. M. LeBlanc, K. T. Sheets, R. W. Fox and P. Gatenholm, *Mater. Sci. Eng., C*, 2011, **31**, 43–49.
203 Y. Hu, Y. Zhu and X. Zhou, *J. Mater. Chem. B*, 2016, **4**, 1235–1246.
204 D. Y. Zaki, E. M. Safwat, S. M. Nagi, H. N. Salem, T. M. Hamdy, L. M. Moharam, M. L. Hassan and E. M. A. Hamzawy, *Carbohydr. Polym. Technol. Appl.*, 2021, **2**, 100035.
205 T. Dvir, B. P. Timko, D. S. Kohane and R. Langer, *Nat. Nanotechnol.*, 2011, **6**, 13–22.
206 S. Weiner and H. D. Wagner, *Annu. Rev. Mater. Sci.*, 1998, **28**, 271–298.
207 F. Nudelman, K. Pieterse, A. George, P. H. H. Bomans, H. Friedrich, L. J. Brylka, P. A. J. Hilbers, G. de With and N. A. J. M. Sommerdijk, *Nat. Mater.*, 2010, **9**, 1004–1009.
208 U. G. K. Wegst, H. Bai, E. Saiz, A. P. Tomsia and R. O. Ritchie, *Nat. Mater.*, 2015, **14**, 23–36.
209 S. Sprio, S. Panseri and M. Montesi, *J. Eur. Ceram. Soc.*, 2020, **40**, 1717–1727.
210 X. Wang, J. Fang, W. Zhu, C. Zhong, D. Ye, M. Zhu, X. Lu, Y. Zhao and F. Ren, *Adv. Funct. Mater.*, 2021, **31**, 2010068.
211 F. Liu, B. Wei, X. Xu, B. Ma, S. Zhang, J. Duan, Y. Kong, H. Yang, Y. Sang, S. Wang, W. Tang, C. Liu and H. Liu, *Adv. Healthcare Mater.*, 2021, **10**, 2001851.
212 J. Sundberg, C. Gotherstrom and P. Gatenholm, *Biomed. Mater. Eng.*, 2015, **25**, 39–52.
213 T. Selorm and S. Prakit, *Appl. Mater. Today*, 2018, **11**, 34–49.
214 Z. Cheng, Z. Ye and A. Natan, *ACS Appl. Mater. Interfaces*, 2019, **11**, 42486–42495.
215 P. M. Favi, S. P. Ospina, M. Kachole, M. Gao, L. Atehortua and T. J. Webster, *Cellulose*, 2016, **23**, 1263–1282.
216 P. Basu, N. Saha, R. Alexandrova, B. Andonova-Lilova, M. Georgieva, G. Miloshev and P. Saha, *Int. J. Mol. Sci.*, 2018, **19**, 3980.
217 N. Mitrousis, A. Fokina and M. S. Shoichet, *Nat. Rev. Mater.*, 2018, **3**, 441–456.
218 M. Mastrogiacomo, S. Scaglione, R. Martinetti, L. Dolcini, F. Beltrame, R. Cancedda and R. Quarto, *Biomaterials*, 2006, **27**, 3230–3237.
219 Y. Huang, J. Wang, F. Yang, Y. Shao, X. Zhang and K. Dai, *Mater. Sci. Eng., C*, 2017, **75**, 1034–1041.
220 C. Rey, C. Combes and C. Drouet, *Osteoporosis Int.*, 2009, **20**, 1013–1021.
221 M. Ojansivu, A. Rashad, A. Ahlinder, J. Massera, A. Mishra, K. Syverud, A. Finne-Wistrand, S. Miettinen and K. Mustafa, *Biofabrication*, 2019, **11**, 035010.
222 M. Sukul, T. B. Nguyen, Y. K. Min, S. Y. Lee and B. T. Lee, *Tissue Eng., Part A*, 2015, **21**, 1822–1836.
223 P. Basu, N. Saha and P. Saha, *Int. J. Polym. Mater. Polym. Biomater.*, 2019, **68**, 134–144.
224 R. E. Abouzeid, R. Khiari, D. Beneventi and A. Dufresne, *Biomacromolecules*, 2018, **19**, 4442–4452.
225 J. Guo, Q. Li and R. Zhang, *Biomacromolecules*, 2022, **23**, 877–888.
226 X. Zhu, T. Chen, B. Feng, J. Weng, K. Duan, J. Wang and X. Lu, *ACS Biomater. Sci. Eng.*, 2018, **4**, 3534–3544.
227 H. Oliveira, S. Catros and O. Castano, *Acta Biomater.*, 2017, **54**, 377–385.
228 H. Jafari, M. Shahrousvand and B. Kaffashi, *ACS Biomater. Sci. Eng.*, 2018, **4**, 2484–2493.
229 X. Zhang, X. Yin, J. Luo, X. Zheng, H. Wang, J. Wang, Z. Xi, X. Liao, J. O. Machuki, K. Guo and F. Gao, *ACS Biomater. Sci. Eng.*, 2019, **5**, 294–307.
230 Q. Chen, R. P. Garcia, J. Munoz, U. Perez de Larraya, N. Garmendia, Q. Yao and A. R. Boccaccini, *ACS Appl. Mater. Interfaces*, 2015, **7**, 24715–24725.
231 P. Mohammadi, J. A. Gandier, Nonappa, W. Wagermaier, A. Miserez and M. Penttila, *Adv. Mater.*, 2021, **33**, e2102658.
232 Y. Qi, Z. Cheng, Z. Ye, H. Zhu and C. Aparicio, *ACS Appl. Mater. Interfaces*, 2019, **11**, 27598–27604.

233 P. Mujuan, H. Yinghong and M. Fansu, *Eur. Polym. J.*, 2020, **122**, 109365.
234 Q. Xu, M. Xu, C. Lin, Q. Zhao, R. Zhang, X. Dong, Y. Zhang, S. Tian, Y. Tian and Z. Xia, *Adv. Sci.*, 2019, **6**, 1902043.
235 M. Wu, P. Wu and L. Xiao, *Int. J. Biol. Macromol.*, 2020, **162**, 1627–1641.
236 R. Singla, S. Soni and P. M. Kulurkar, *Carbohydr. Polym.*, 2017, **155**, 152–162.
237 J. Leppiniemi, P. Lahtinen and A. Paajanen, *ACS Appl. Mater. Interfaces*, 2017, **9**, 21959–21970.
238 J. Wu, N. Yin and S. Chen, *Cellulose*, 2019, **26**, 2513–2528.
239 L. L. Demer and Y. Tintut, *Circulation*, 2008, **117**, 2938–2948.
240 M. Parvinzadeh Gashti, M. Stir, M. Bourquin and J. Hulliger, *Cryst. Growth Des.*, 2013, **13**, 2166–2173.
241 S. Yao, B. Jin, Z. Liu, C. Shao, R. Zhao, X. Wang and R. Tang, *Adv. Mater.*, 2017, **29**, 1605903.
242 R. Zhao, B. Wang and X. Yang, *Angew. Chem., Int. Ed.*, 2016, **55**, 5225–5229.
243 J. Klesing, A. Wiehe, B. Gitter, S. Grafe and M. Epple, *J. Mater. Sci.: Mater. Med.*, 2010, **21**, 887–892.
244 S. A. Noorian, N. Hemmatinejad and J. A. R. Navarro, *J. Inorg. Biochem.*, 2019, **201**, 110818.
245 A. Fakhri, S. Tahami and P. A. Nejad, *J. Photochem. Photobiol., B*, 2017, **175**, 83–88.
246 M. M. Abeer, M. C. I. Mohd Amin and C. Martin, *J. Pharm. Pharmacol.*, 2014, **66**, 1047–1061.
247 R. Mori, T. Nakai and K. Enomoto, *Clin. Orthop. Relat. Res.*, 2011, **469**, 600–606.
248 J. Supramaniam, R. Adnan, N. H. M. Kaus and R. Bushra, *Int. J. Biol. Macromol.*, 2018, **118**, 640–648.
249 T. S. Anirudhan, S. S. Nair and V. C. Sekhar, *J. Membr. Sci.*, 2017, **539**, 344–357.
250 H. Luo, H. Ao and G. Li, *Curr. Appl. Phys.*, 2017, **17**, 249–254.
251 A. Nishiguchi and T. Taguchi, *Biomacromolecules*, 2019, **20**, 1385–1393.
252 M. R. McClung, P. Geusens, P. D. Miller, H. Zippel, W. G. Bensen, C. Roux, S. Adami, I. Fogelman, T. Diamond, R. Eastell, P. J. Meunier, R. D. Wasnich, M. Greenwald, J. Kaufman, C. H. Chesnut and J. Reginster, *N. Engl. J. Med.*, 2001, **344**, 333–340.
253 L.-H. Fu, C. Qi, Y.-J. Liu, W.-T. Cao and M.-G. Ma, *Sci. Rep.*, 2018, **8**, 8292.
254 A. Salama, M. El-Sakhawy and S. Kamel, *Int. J. Biol. Macromol.*, 2016, **93**, 1647–1652.
255 F. V. Ferreira, C. G. Otoni, K. J. De France, H. S. Barud, L. M. F. Lona, E. D. Cranston and O. J. Rojas, *Mater. Today*, 2020, **37**, 126–141.
256 D. Klemm, E. D. Cranston, D. Fischer, M. Gama, S. A. Kedzior, D. Kralisch, F. Kramer, T. Kondo, T. Lindström, S. Nietzsche, K. Petzold-Welcke and F. Rauchfuß, *Mater. Today*, 2018, **21**, 720–748.
257 S. Gorgieva and J. Trček, *Nanomaterials*, 2019, **9**, 1352.
258 P. Shen, Q. Tang, X. Chen and Z. Li, *Carbohydr. Polym.*, 2022, **290**, 119462.
259 W. Liu, H. Du, M. Zhang, K. Liu, H. Liu, H. Xie, X. Zhang and C. Si, *ACS Sustainable Chem. Eng.*, 2020, **8**, 7536–7562.